Paleo-environmental Reconstructions of the Paleocene Equatorial Atlantic Ocean based upon Biomarkers and Dinoflagellate Cysts

Mike Nicolai

(4290437)

1st supervisor	**:**	dr. Peter Bijl
2nd supervisor	**:**	prof. dr. Appy Sluijs
Datum	**:**	27/08/2016

Abstract

In contrast to the warm early-Eocene "hothouse" conditions (~56-51 Ma), which was subject to comparable CO_2 concentrations as predicted for our future assuming unabated anthropogenic fossil fuel consumption (Archer, 2005), the "greenhouse" mid-Paleocene (~62-58 Ma) has been barely investigated. The latter despite the potential similarities with the present-day climate system in terms of atmospheric pCO_2. Uncertainty about the presence of substantial polar ice-sheets during the mid-Paleocene episode and the warming which led to this "hothouse", particularly for the data-lacking tropics, remains significant. To gain new insights in this matter, this study presents reconstructions of the marine paleo-environment, paleo-temperatures, and sea-level fluctuations. These reconstructions were done by investigating palynomorph assemblages (notably organic-walled dinoflagellate cysts) and applying paleo-thermometers TEX_{86} and MBT/CBT on equatorial Paleocene sediments from ODP site 959D, offshore Ivory Coast (west-Africa). Unfortunately, the biomarker analyses did not result in any quantitative reconstructions for land and sea surface temperature as the sediments were too mature. Dinocyst events however allowed the existing stratigraphic age model to be considerably improved for the Paleocene part of the model. Furthermore the combined results from the applied palynological proxies and results of related studies, for instance $\delta^{18}O$ isotope trends as detailed by Westerhold et al. (2011), reflect that the most plausible pronounced continental ice-sheet presences are suspected for the mid-to-late Paleocene, although supporting evidence is thin. These combined results also imply a prevailing open marine to pelagic setting at Paleocene site 959, where paleo-productivity was predominantly controlled by wind-induced upwelling, riverine input, stratification and sea-level shifts.

Contents

1. Introduction

Atmospheric CO_2 concentrations will increase significantly in the coming centuries as a consequence of ongoing anthropogenic carbon dioxide emissions, which affect Earth's climate. The exact responses of pCO_2 forcing on climate however are difficult to project to the future due to complex feedbacks in the climate system. This results in large uncertainties in the climate sensitivity, which might decrease economic stability and societal welfare (Solomon et al., 2007). One way to improve accuracy in future climate scenarios is by looking into eras of Earth's history that are characterized by CO_2 concentrations similar to those expected for our future. The early Eocene (~50 Ma) is such a "hothouse" climate (Hollis et al., 2014) where atmospheric pCO_2 reached levels at least comparable to those expected for the future, assuming unabated carbon emission scenarios (Archer, 2005). Due to the similarity between pCO_2 conditions in the early Eocene and those projected for the future, this "hothouse" period has been intensively studied over the past twenty years. However the warming which led to this climate state and the mid-Paleocene climate minimum from when it potentially started, despite the potential similarity in greenhouse gas values and ice sheets to today (Ruddiman, 2014; Westerhold, et al., 2011), has barely been investigated. Reasons for this may lie in a general paucity of complete sedimentary records that capture this time interval. Recently, high-resolution (benthic foraminiferal oxygen- and carbon isotope) sedimentary records for the Paleocene became available (Westerhold et al., 2011), which reflect a combination of deep-sea temperature changes and, if present, changes in ice volume (Ruddiman, 2014). Unfortunately, it is as yet unknown to what extent the isotope record represents mostly a temperature or an ice volume signal, because it is unclear whether there were significant amounts of continental ice present during the Paleocene. Additional evidence for the suspected presence of ice sheets in the cold mid-Paleocene will significantly improve our knowledge of the climate sensitivity to relatively low pCO_2 conditions, since important climate feedbacks such as albedo are associated with ice sheets (Ruddiman, 2014). Furthermore we lack insights in land and sea surface temperature [LaSST] gradients and the paleo-environment during the Paleocene as well: particularly data from equatorial regions is notoriously lacking. LaSST reconstructions from the Paleocene equatorial region would greatly improve our insight in the distribution of heat during the Paleocene, in the context of Eocene "hothouse" conditions.

The aims of this study are to reconstruct paleo-environmental changes of the mid-Paleocene climate minimum and the subsequent transition towards the early Eocene 'hothouse' for the equatorial region in more detail. To achieve this firstly the results of sea and land surface temperature reconstructions for the Paleocene from ODP Site 959 offshore Ivory Coast are presented, which were derived by applying the combination of biomarkers TEX_{86} and MBT/CBT on sedimentary records obtained from that location. These reconstructions may then be used to analyse the temperature distribution trends and the influence of temperature on paleo-environment in the equatorial Atlantic Ocean region for the Paleocene. Regrettably no land and sea surface temperatures were reconstructed for the studied site, due to insufficient biomarker concentrations within the investigated sediments. Furthermore the biostratigraphy is improved for the mid-Paleocene and the transition towards the early Eocene by analysing fossilised dinocyst assemblages captured in the sedimentary records from the same ODP Site. This in turn is used to reconstruct the tropical continental shelf paleo-environment of the Paleocene in terms of oceanological setting, productivity and sea level fluctuations, hereby applying the dinocyst grouping as defined by Guasti (2005) and Sluijs & Brinkhuis (2009). The sea level shifts are analysed, in order to derive an eventual presence of substantial mid-Paleocene continental ice sheets. This is used to investigate whether the high resolution records of Westerhold et al. (2011) probably reflect mostly an ice volume or temperature signal. Ultimately these findings may be used to improve accuracy in future climate scenarios.

2. Material

2.1. Sampling Site 959

All 33 samples that were used for this research were obtained from sedimentary records stored in the Bremen Core Repository. However these records were originally acquired by the Ocean Drilling Program [ODP] Leg 159 at coring site 959 (geographic coordinates: 3°37.656'N, 2°44.149'W) between the 14th and 24th of January in 1995. This specific site lies on the northern slope of the marginal ridge of the Ghana-Côte d'Ivoire Transform Margin (as shown in figure 1B) at a depth of approximately 2100 m and is located roughly 150 km south of the Ghanese coast. This margin separates two marine basins, i.e. the Deep Ivorian Basin and the Guinea Abyssal Plain (as illustrated in figure 1). Four holes were drilled, 959A to 959D. From site 959 hole D a number of 78 cores were recovered by the ODP of which 8 cores are selected for this study. The specific cores used are core 159-959D-42R through -49R and these represent the drilling interval of roughly 802.6 to 879.9 meters below sea surface [mbsf] (see figure 1). These sedimentary records from hole 959D were chosen due to the fact that it is up till now one of the leading examples that captured the equatorial Paleocene epoch relative completely (Mascle, Lohmann, & Clift, 1996).

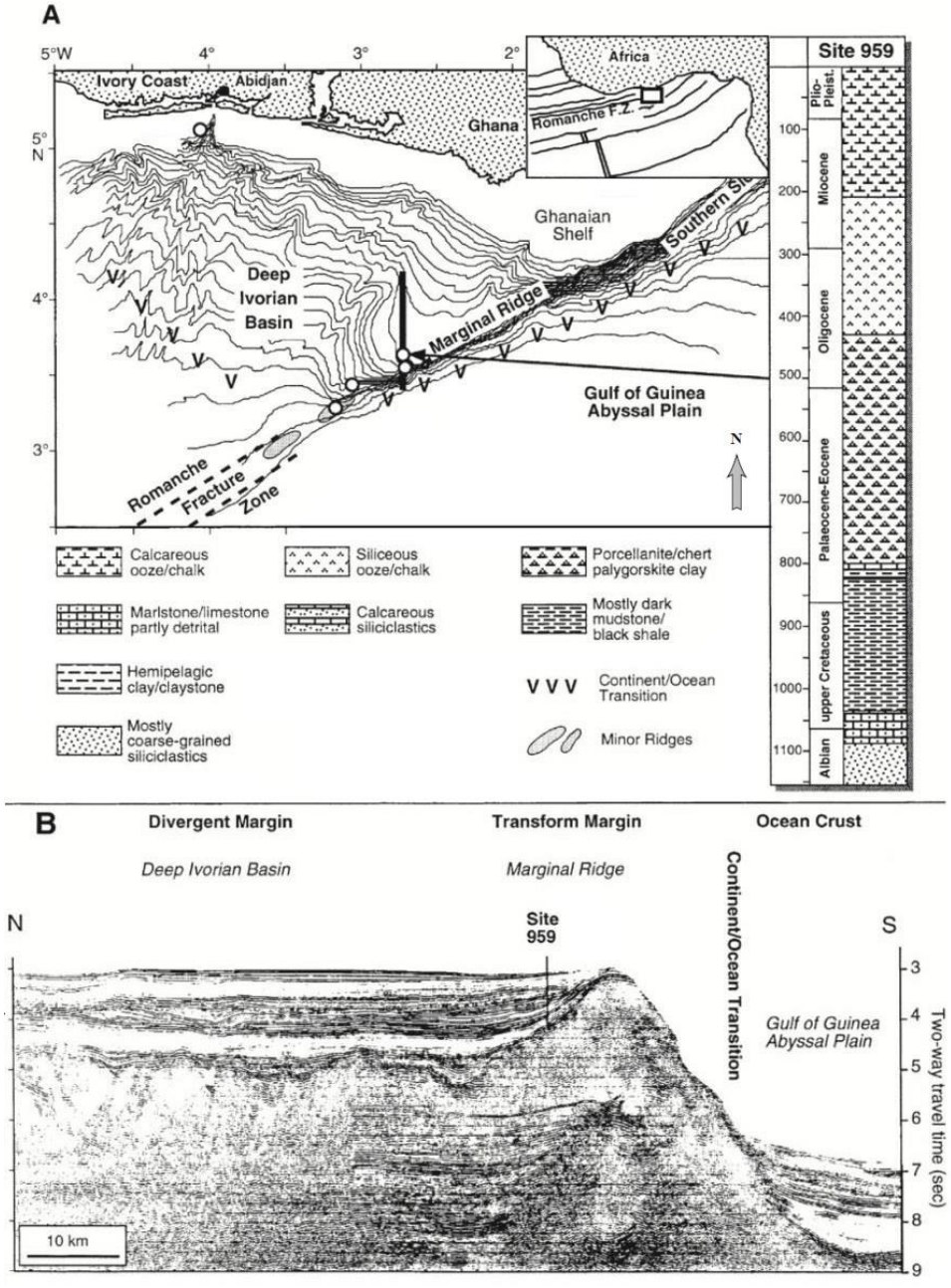

Figure 1: Present day site-location of ODP site 959 on the Côte d'Ivoire-Ghana Marginal ridge – Africa. Dark grey lines indicate lines of iso-depths, white areas reflect submerged regions and grey areas illustrate land masses. Edited from Wagner (2002).

2.2. Geological History

Site 959 borders the Côte d'Ivoire-Ghana Transform Margin on the northern side (as shown in figure 1B). This so-called Marginal Ridge is the result of significant tectonic spreading in the early to late Cretaceous, which led to transform motions between local continental and oceanic plates (Wagner, 2002). Together with persistent subsidence along the Transform Margin this eventually resulted in an predominantly open ocean connection between the Deep Ivorian Basin and the Guinea Abyssal Plain in the Paleocene, and allowed continued deep-water circulation (see figure 2) (Wagner, 2002). Oboh-Ikuenobe (1997), who reconstructed the paleo-bathymetry for site 959, suggested middle to lower bathyal conditions throughout the Paleogene and even nearly abyssal levels in the early Eocene. Based on benthic foraminifers, similar water depths close to the lower limit of an oxygen minimum zone [OMZ] were implied by (Bignot, 1998). A significant OMZ was also proposed for the Deep Ivorian Basin by Wagner (2002) for the early Paleocene.

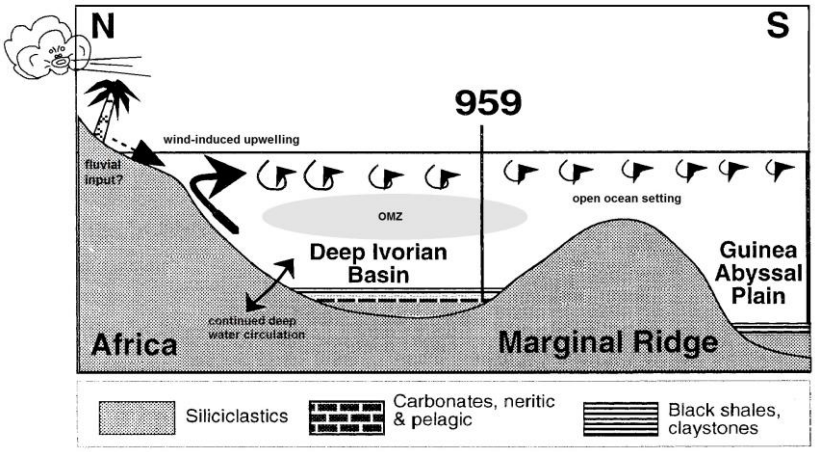

Figure 2: Graphical depiction of the suspected geological setting in the proximity of site 959 at Paleocene times. Modified from Wagner (2002).

Figure 3: Geographical map illustrating the paleo-location of site 959D around 60 Ma in relation to Africa, South America and the Atlantic Ocean. The paleo-latitudes and longitudes are also included. Image modified from software-package PAMS.

The presumed Paleocene geographical position of site 959D is approximated directly south of the equator (as depicted in figure 3) at a latitude of ~4.5° S (PALEOMAP Project, 2000). In modern times, at and near the equator as well as coastal settings, upwelling of deep water that is induced by the wind is frequently observed (Garrison, 2013). This suspected wind-induced upwelling of nutrient-enriched waters near the Transform Margin and in the Deep Ivorian Basin (as illustrated in figure 2 is supported by the identification of a significant band of bio-siliceous sediments in the equatorial Paleogene Ocean near site 959. (Wagner, 2002). According to Wagner (2002) these sediments also imply situations of free flowing equatorial surface waters through the ocean basins in the Paleocene.

The deposition of sediments and organic matter at site 959 was most likely a combined signal of transport of the African continental shelf and a local (pelagic) signal, although it is hard to distinguish between these two (Frieling et al., 2016).

2.3. Core Sediment and Recovery

ODP Site 959 hole D contains sediments which range from an early Cretaceous to Miocene age (Mascle et al., 1996). According to Mascle et al. (1996) the lithology found in the investigated section consists mainly of clay- and siltstone (see figure 1A and 4). Core recovery varies greatly, ranging from less than 10 % to 100 % (as demonstrated in figure 7 and 8). Core 42R was recovered for 42.6 %, whereas core 43R and 44R had 100% recovery. While core 45R to 47R show large gaps in their recovery (10 to 20 % recovery). Hereafter recovery values improved significantly, from core 48R and core 49R respectively 85 and 90 per cent was retrieved. In addition to this the majority of the studied core sediments appear to illustrate cyclic dark-light alternations in colour (as shown in figure 7, 8 and 9), which are presumably a result of changes in the composition of the sediment. The core photographs showing the darkest discolorations are likely the cores that are relatively rich in organic matter (Mascle et al., 1996).

2.4. Initial Age model

Mascle et al. (1996) stated that cores 42R and 43R contain certain biostratigraphically important calcareous nannofossils such as *Discoaster multiradiatus* and *Rhomboaster bitrifida,* which enabled some degree of preliminary age determination (see table 2). In core 42R the onset of the Paleocene–Eocene Thermal Maximum [PETM] was identified by Frieling et al. (2016) at a depth of 804.09 mbsf., applying the findings of Gradstein et al. (2012). The PETM marks the 55.96 Ma boundary between the Paleocene and Eocene epochs (Westerhold et al., 2008). Furthermore core depth 44R-3 90-91 cm down to and including 49R are lacking in calcareous nannofossils, and yield an incomplete and low intensity range of magnetization, which complicates paleo-magnetostratigraphic inferences. Additionally, the record contains only sporadically agglutinated *foraminifera* assemblages that made precise preliminary age determinations impossible without the use of palynology (Mascle et al., 1996). The Cretaceous-Tertiary [K-T] boundary, and thus the start of the Paleocene epoch, was identified in core 49R on the basis of pollen analysis in this same publication, based on terrestrial palynomorph stratigraphy. Dinoflagellate cyst events captured in the investigated sediments in combination with stratigraphic calibrations of other studies are in this research used to provide additional age constraints for the Paleocene part of the record (as shown in table 2).

In addition 33 samples were selected from core 959D sections 42R to 49R (see table 2 and figure 7 - 9), which, based on the initial stratigraphic age model, should capture the entire Paleocene between the K—Pg boundary to the Paleocene-Eocene Thermal Maximum (including some degree of overlap).

3. Methods

3.1. Palynology

3.1.1. Background

The aimed paleo-environmental reconstructions were partly based on a palynological study focussing on fossilised dinoflagellates cysts, or in short and more commonly referred to as dinocysts. The use of dinocysts was chosen since dinoflagellates are known to be mostly marine unicellular planktic organisms, which are and were widely spread throughout their long history of evolution (Garrison, 2013). Numerous modern and extinct species produce a highly resistant cyst during their motile stage, that is generally well preserved in marine sediments for instance (Gradstein et al., 2012). Investigation of these marine cysts has therefore been successfully adopted in multiple modern palynological studies for reconstructing among others stratification of water masses, sea level shifts and sea surface productivity (Guasti, 2005).

3.1.2. Palynological Preparation

Standard palynological processing protocols (e.g., Sluijs et al., 2003) were applied on the whole sequence of 33 samples in the GML laboratory, which is located on the Utrecht University campus *De Uithof*. This was done in order to prepare the samples for light microscopy.

At first from each of the freeze-dried samples six to ten grams was taken, scraped to in situ material and then crushed to grain size fragments of roughly half a centimetre. The crushed samples were weighted and thereafter stored. *Lycopodium clavatum* tablets with a known concentration of spores per tablet (n = 20848 ± 688 and n = 9666 ± 213) were added to each of the samples to enable quantification during palynological analysis as described by Stockmarr (1971). Subsequently the samples were moisturised with the concentrated wetting agent *Agepon* and then diluted 30% hydrochloric acid [HCL] was added until no further reaction could be observed while stirring. Water was now added and poured off twice before finally being added again. Then the samples were centrifuged for five minutes and thereafter drained again of the water to remove the dissolved calcium carbonates. Now diluted 40% hydrofluoric acid [HF] was added step by step until the jar was half filled, in order to remove all silica compounds from the samples. The sample solutions were now stored overnight in a fume hood cabinet. Thereafter all the samples were placed in the shaking device for two hours to ensure complete reactions with the HF, and then refilled with water. Next the fluid from the samples was poured off as much as possible, an overload HCL was added again. Then water was added and the samples were centrifuged a second time for five minutes. The samples were now sieved using filters with a mesh size of 250 μm to remove large non-useable particles. The residue under the filter was captured with water. This residue was then filtered using a sieve with mesh size 10 μm and the material that remained on the filter was now captured on a porcelain scale using squirts of water. Next the porcelain scale containing the sample was placed in an ultrasonic bath for approximately five minutes to disintegrate larger clumps of soil and eventually aid creating clean slides. The previous 10 μm filter and porcelain scale capture step was then repeated again, before the porcelain scale was placed in the ultrasonic bath another time for 30 seconds. Thereafter the remainder of the sample was captured in glass test-tubes, water was added and the samples were centrifuged for five minutes again. Subsequently the samples were decanted and then five drops of glycerine water was added before the samples were poured off in mini test-tubes. Next the samples were centrifuged another time with the same duration and decanted again. Then one or two drops from the sample was or were taken to prepare two slides per sample for light microscopy using glycerine gelatine. Finally after the slides were congealed, they were sealed using nail varnish and were stored to dry. The dry slides were then used for palynological analysis.

3.1.3. Palynological Analyses

Palynological analyses were performed on all prepared slides using an Olympus light microscope, model CX21FS1. Of each sample one or two slides were examined at 400x magnification, or at a zoom of 1000x when studying certain unclear specimens of dinocysts. In addition several known and unknown types of dinocysts and palynomorphs were photographed using a Leica light microscope (model: 020-519.511 DMLB 100T), which was equipped with a Leica camera of the type MC120 HD, and are detailed in Appendix C and D.

Each sample was systematically counted till 200 determinable specimens of dinoflagellate cysts were reached. However in some cases one slide did not contain 200 identifiable dinocysts, here both slides of a sample were completely counted on account of maximising the number of cysts as much as possible for analysation. When 200 specimens had been counted, the rest of the slide was scanned globally in order to find yet undetected key dinocyst species. Furthermore counts for epicystal dinocysts were divided by two, to prevent over-counting. Next to this every dinocyst was counted at species level where possible, otherwise at genus level. Appendix B presents the list of all encountered dinocysts species and genera. In addition while counting up to 200 dinocysts, distinct palynomorphs, pollen, spores, acritarchs and foram linings were also taken into account and numbered, although not at species but at a more general level. Subsequently the in this study used definition of acritarchs is as follows; small (<30 μm) dinoflagellate resembling cysts which lack a distinct recognisable archaeopyle.

Ultimately this acquired dataset of dinocyst assemblages was firstly used to attempt improving the existing age model on the basis of first and last dinocyst occurrences and thereafter, with the improved age model, the existing biostratigraphic framework. The result of this is demonstrated in figure 7. The assemblages were also used to signify trends in the tropical marine paleo-environment of the Paleocene in terms of oceanological setting, productivity and sea level fluctuations.

3.1.4. Palynological Tools for Paleo-environmental Reconstructions

For setting up a reliable model for reconstructing the equatorial paleo-environment of site 959, specific taxa, groups or complexes of dinoflagellates and palynomorphs were selected from the established assemblages to be used as palynological proxies. Hereby following the grouping as defined by Guasti (2005) and Sluijs & Brinkhuis (2009). This was done since earlier studies have increased the confidence that these taxa, groups and complexes (see table 1) may in fact be related to alternating paleo-oceanological settings, paleo-productivity and past sea level fluctuations on the basis of empirical evidence as detailed in this subchapter. Note that some of these relations are developed on the basis of wide stable continental shelf conditions (e.g. figure 4). As already discussed the tectonic setting at site 959 is fundamentally different from such a continental shelf (see figure 2) (Wagner, 2002). Additionally the deposition of organic matter was most likely a combined signal of transport of the African continental shelf and a local signal, although it is hard to distinguish between these two (Frieling et al., 2016). The by Guasti (2005) and Sluijs & Brinkhuis (2009) proposed paleo-environmental implications of the proxies can therefore not all be adopted one to one, which will be discussed in chapter 4.

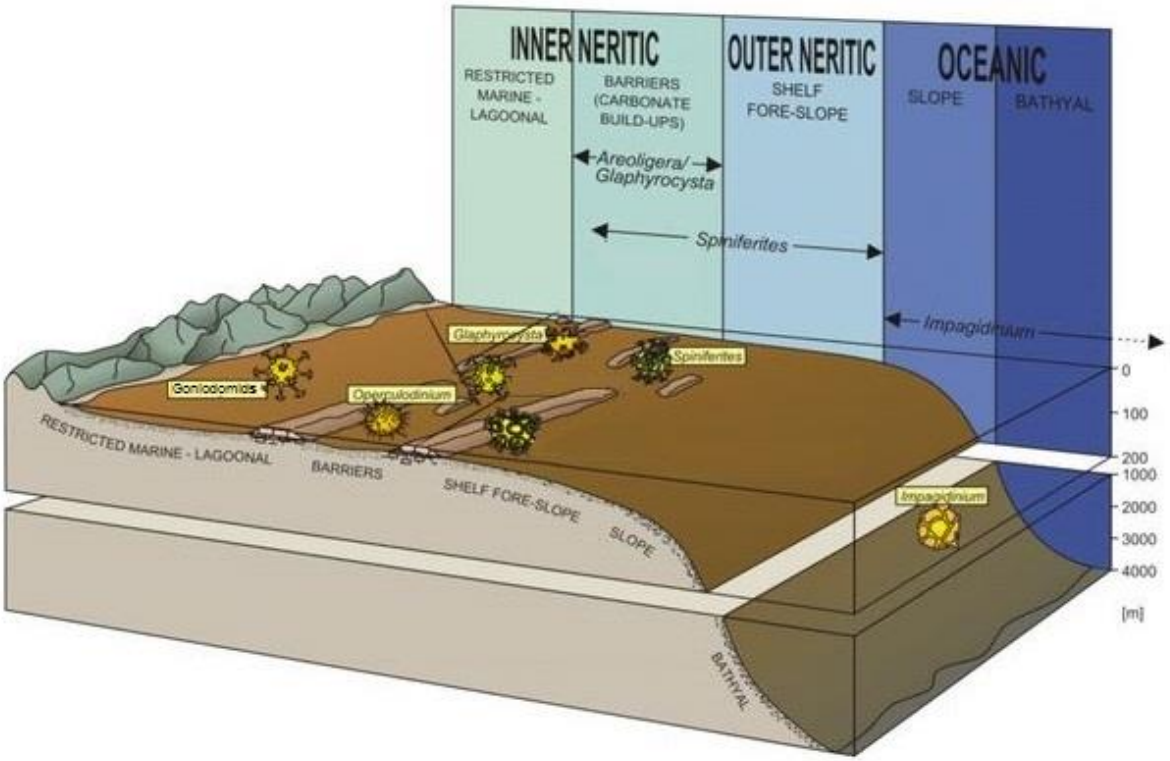

Figure 4: Schematic representation of a wide hypothetical continental shelf, demonstrating different marine settings and the associated preferences of several dinocyst taxa. This figure was added to help illustrate the theory behind the S:A ratio used for this research. The figure is modified from Sluijs et al., Earth-Science reviews 68, p281, 2005.

Paleo-oceanological Setting Indicators

Sluijs & Brinkhuis (2009) illustrated that increased numbers of the dinocyst genus of *Apectodinium spp*. may reflect a signal of elevated SST, nutrient rich shallow marine settings when *Apectodinium* is assumed as an heterotrophic genus and/or waters with reduced salinities. Furthermore cysts of *Operculodinium spp.* were often recorded in more offshore settings due to transportation and are considered as indicators of an open marine environment and transport (Eshet et al., 1992; Brinkhuis, 1994; Pross & Brinkhuis, 2005; Slimani et al., 2010). Besides that relative abundancies of the *"Cordosphaeridium fibrospinosum* group*"* over the total of encountered dinocysts as used by Houben (2008) (represented in this study by *Cordosphaeridium spp.*, *Damassidinium spp.*, *Fibrocysta spp.*, *Muratodinium spp*. and *Thalassisphora spp*.) is linked with enhanced stratification or even brackish conditions in the water column (Brinkhuis, 1994; Houben, 2008; Pross &

Brinkhuis, 2005; Sluijs et al., 2005). Next to this peaks in specimens of the combined *Eocladopyxis spp*., *Polysphaeridium spp*. and *Homotryblium spp*., commonly termed as the Goniodomid group, are associated with low latitude hypo- or hypersaline lagoon-like settings (see figure 4) (Bradford & Wall, 1984; Reichart et al., 2004). Subsequently abundances of Goniodomid *Polysphaeridium zoharyi* are also related to an hyperstratified water column with lagoonal conditions in the open ocean (Reichart et al., 2004). Furthermore, evidence strongly suggests that the *Senegalinium* group (consisting of most of the spectrum of the Peridiniod cyst genera, namely *Senegalinium spp*., *Phtanoperidinium spp*., *Deflandrea spp., Cerodinium spp., Palaeocystodinium spp., Spinidinium spp.* and other related cysts genera) were able to cope with low salinity environments as well, and appeared to thrive when nutrient concentrations were high (Brinkhuis & Zachariasse, 1988; Firth, 1996). Furthermore the taxa *Impagidinium spp*. was assumed to illustrate situations where open marine oligotrophic settings prevailed (as shown in figure 4) (Guasti, 2005), connecting with studies that looked into modern taxa of *Impagidinium* (Brinkhuis & Zachariasse, 1988; Crouch et al., 2003). High abundances of these types of cyst could therefore imply enhanced open ocean influences.

Paleo-productivity Proxies

Besides being used as paleo-oceanological setting indicators, both *Senegalinium* as well as *Apectodinium* are also associated with high nutrient availability (resp., Sluijs & Brinkhuis, 2009; Firth, 1996) and were therefore used as paleo-productivity proxies as well. Furthermore the "classical" ratio of cysts with a Peridinioid [P] over Gonyaulacoid [G] type of tabulation was also applied to study paleo-productivity, hereby following Almogi-Labin et al. (1993). In this study it is strongly suggested that fluctuations in productivity influence the ratio between the mainly heterotrophic P and the autotrophic G dinocysts as a direct consequence of nutrient availability. For this ratio all encountered dinocysts with a P or G type tabulation were used from the generated dataset. The P over G ratio was then calculated for each sample using the equation:

(1) $$[\text{P} - \text{G ratio}] = \frac{\text{P}}{(P+G)}$$

Where P and G reflect the total number of dinocysts with respectively Peridinioid and Gonyaulacoid tabulation identified in a sample. Subsequently low values relate to low sea surface productivity, whereas high values reflect enhanced sea surface productivity (e.g., Guasti, 2005). Furthermore quantification of the absolute number of dinoflagellates in a sample was done with the *Lycopodium* method (e.g., Stockmarr, 1971). This so-called Absolute Dinocyst Abundance [ADA], which depicts the absolute quantity of dinocysts per gram sample on the basis of Lycopodium pollen, was determined using the following formula:

(2) $$\text{Abs. Dinocyst Abundance [ADA]} = \left(\frac{\left(\frac{\text{nD}}{nL}\right) * tL}{m}\right)$$

Here nD and nL represent the absolute number of encountered dinoflagellates and *Lycopodium* pollen respectively in a sample, tL the total quantity of *Lycopodium* added to the sample with the *Lycopodium* tablet and m the total weight of the processed sample in grams. Additionally the ADA was implemented to quantify the number of dinocysts per gram sample, which in turn was used to illustrate paleo sea surface productivity trends (see figure 9) (Sluijs & Brinkhuis, 2009). Another method that was chosen to demonstrate these trends was the study of Absolute fossilised organic benthic Foraminifera linings Abundance [AFA] (e.g., Frieling et al., 2016). The AFA was also calculated using equation (3), but instead of using nD, the absolute number of encountered Foram linings [nF] was filled in. Furthermore an increase in pollen and spores may suggest enhanced fluvial or aeolian terrestrial run off into coastal surface waters (Garrison, 2013), such as at the African continental shelf.

Past Sea Level Indicators

The *Areoligera complex [cpx.]* (consisting of *Areoligera spp*., *Glaphyrocysta spp*. and *Adnatosphaeridium spp*.) shows a strong positive correlation with high energy inner neritic environments, whereas on the other hand the generalistic *Spiniferites cpx.* (*Achomasphaera spp*., *Hafniasphaera spp*. and *Spiniferites spp*.) tends to favour outer neritic conditions (as depicted in figure 4) (Brinkhuis, 1994; Pross & Brinkhuis, 2005). Correlating these two genera formed the basis for the development of the here used *Spiniferites* [S] to *Areoligera cpx.* [A] ratio, which is suggested to reflect relative changes in sea level on a wide stable continental shelf with a gradual slope (Sluijs et al., 2008). The S:A ratio was calculated per sample using the following comparison;

(3) $$[S:A\ ratio] = \frac{S}{(S+A)}$$

Here S and A depict the total of encountered specimens of the *Spiniferites* and *Areoligera* complex respectively in a sample. Moreover significant decreases in S : A ratio values were assumed to suggest marine regression, while sharp increasing values would emphasize towards transgressive events.

Table 1: Palynological grouping of dinoflagellate cysts based on concurrent paleo-environmental implications.

Palynological Group	Dinoflagellate "members"
Apectodinium	*Apectodinium spp.*
Areoligera complex	*Areoligera spp*., *Glaphyrocysta spp*. and *Adnatosphaeridium spp*.
***Cordosphaeridium fibrospinosum* group**	*Cordosphaeridium spp*., *Damassidinium spp*., *Fibrocysta spp*., *Muratodinium spp*. and *Thalassisphora spp*.
G - Group	All encountered dinocysts with a Gonyaulacoid type tabulation
Goniodomid group	*Eocladopyxis spp*., *Polysphaeridium spp*. and *Homotryblium spp*.
Impagidinium	*Impagidinium spp.*
Operculodinium	*Operculodinium spp.*
P - Group	All encountered dinocysts with a Peridinioid type tabulation
***Senegalinium* group**	*Senegalinium spp*., *Phtanoperidinium spp*., *Deflandrea spp*., *Cerodinium spp*., *Palaeocystodinium spp., and Spinidinium spp.*
Spiniferites complex	*Achomasphaera spp*., *Hafniasphaera spp*. and *Spiniferites spp*.

Lastly the proxy results, core photographs and the in chapter 4.2.1 proposed age model were combined to put figure 8 and 9 together, which in turn were used to signify trends in marine paleo-environmental conditions. Besides this the proxies of this paragraph were compared with the other recorded dinocysts in the data, and in the case possible matches were detected a subgraph was added to figure 8 as well. This was done in order to detect potential new palynological proxies (e.g. subgraph 8i: *Tanyosphaeridium xanthiopyxides*)

3.2. TEX_{86} and MBT/CBT Paleo-thermometers

3.2.1. Background

For the reconstruction and analysation of Paleocene land and sea surface temperatures and its influence on the paleo-environment, a combination of organic geochemistry proxies, namely the biomarkers TEX_{86} and MBT/CBT, were applied on the samples of this study. Both biomarkers are paleo-thermometers that are based upon the distribution of certain (branched) Glycerol Dialkyl Glycerol Tetraethers [GDGTs] and Crenarchaeol [Cren] as shown in figure 5. These GDGTs are found in membrane lipids of certain marine unicellular organisms including Crenarchaeota (Kim et al., 2008; Peterse et al., 2012). The TEX_{86} as well as the MBT/CBT proxy have proven their significant empirical relations with *relative* changes in sea surface- and continental air temperature respectively (Kim et al., 2008; Peterse et al., 2012; Sluijs et al., 2005; Weijers et al., 2006). Nevertheless there remains uncertainty in the reliability of the *absolute* temperature values these proxies point toward (Bijl et al., 2010). Moreover the GDGTs used for TEX_{86} analysis may not solely reflect SST in coastal settings, due to the fact that organic matter produced by coastal benthic organisms might contain some of the GDGT elements hereby disrupting the sea surface signal (Weijers et al., 2006). Hence these proxies were applied to reconstruct *relative* sea surface temperature trends for the equatorial Paleogene.

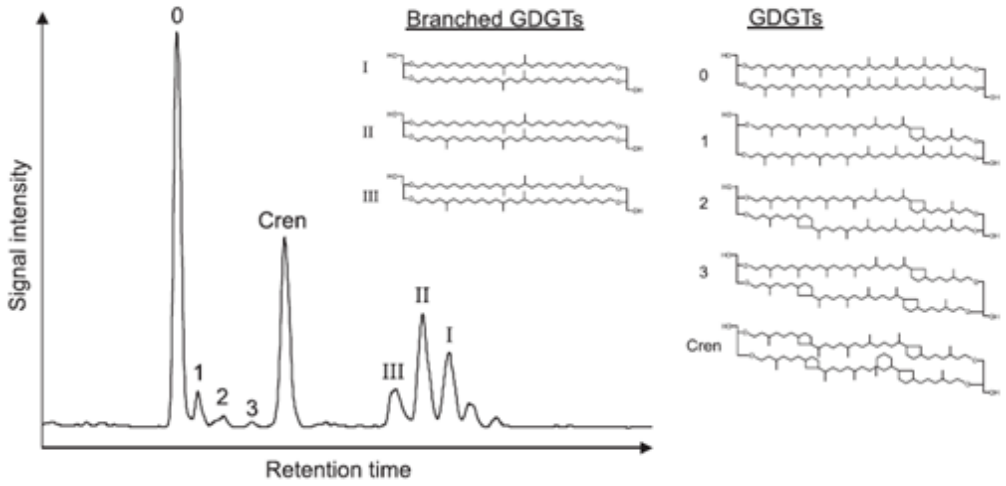

Figure 5: LC-MS base peak chromatogram example, illustrating the presence of the different (branched) GDGT membrane lipids and Crenarchaeol used for TEX_{86} and MBT/CBT temperature analysis. Modified from Hopmans et al. (2004)

3.2.2. Biomarker Preparation

Samples were prepared for organic geochemistry using standard organic geochemistry processing methods, as described by Weijers et al. (2006). This was done in the GML laboratory. Sediments directly overlying the studied interval, showed falling concentrations of GDGTs. Therefore, it was decided to first process a select set of 8 samples.

Similar to palynological processing, first approximately six grams of material was taken from each of the freeze-dried samples, scraped to remove impure sections and then pulverised to powder. Hereafter the powdered samples were weighted and prepared (with diatomaceous earth) for a run in the Accelerated Solvent Extractor type 350 [ASE 350], under standard settings (Weijers et al., 2006) in order to extract the GDGTs. Dichloromethane [DCM] and methanol [MeOH] were utilised as extractants at a ratio of 9:1 (volume DCM : volume MeOH). Subsequently the extracts were dried using a *Turbovap* and thereafter weighted. The extracts were then separated into apolar, ketones and polar fractions using (activated) aluminium oxide column chromatography applying hexane:DCM (9:1 vol. ratio), hexane:DCM (1:1 vol. ratio) and DCM:MeOH

(1:1 vol. ratio) as eluents, respectively. Subsequently all fractions were dried and weighted. In order to analyse the GDGTs, the polar fractions of each sample were now dissolved in hexane:isopropanol (99:1 vol. ratio). This solute was then filtered over a 0.45 μm PTFE filter and transferred with a syringe into 1.5 ml labelled vials at a concentration of 3mg/ml. Finally the solutes were run in the LC-MS, following the calibrations of Hopmans et al. (2015). The resulting chromatograms illustrating the mass spectra of the GDGTs were then used for further geochemical assessment.

3.2.3. Biomarker Analysation

The next step was to analyse whether the eight samples contained adequate quantities of (branched) GDGTs and Crenarcheol in the polar fraction, in order to successfully apply the TEX_{86} and MBT/CBT paleo-thermometers. This was done by integrating the spectral peaks of the chromatograms that the LC-MS has made visible for each geochemically processed sample (e.g. figure 5 and 6). More specifically the peak surface areas were calculated using the computer softwarepackage *Instruments 1 offline*. As experience has shown for these surface areas, they should globally approach the values of the internal laboratory standard that was added to the samples in order to execute trustworthy and accurate biomarker reconstructions. Subsequently in case it was determined that the samples yielded sufficient amounts of the biomarker molecules, the on TEX_{86} and MBT/CBT based (La)SST values were calculated following the methods as defined by Schouten et al. (2002) and de Jonge et al. (2013) respectively. For TEX_{86} the calibrations as proposed by Kim et al. (2010) were applied. More specifically due to the low latitude geographical position of site 959, the TEX_{86}^{H} method with calibration error ≈ 2.5 °C was used, which is recommended for settings where SSTs are expected to be above 15 °C (Kim et al., 2010). The MBT/CBT proxy was calibrated as detailed by Peterse et al. (2012), it produces mean annual air temperatures. Furthermore the Branched Isoprenoid Tetraether versus Crenarchaeol [BIT] index (Hopmans et al., 2004) was applied to investigate the relative terrestrial influence on both paleo-thermometers. According to Hopmans et al. (2004) the terrestrial influence is ought to be minimal when the BIT-index is lower than 0.3.

4. Results and Discussion

4.1. Reconstruction of Paleocene Land and Sea Surface Temperatures

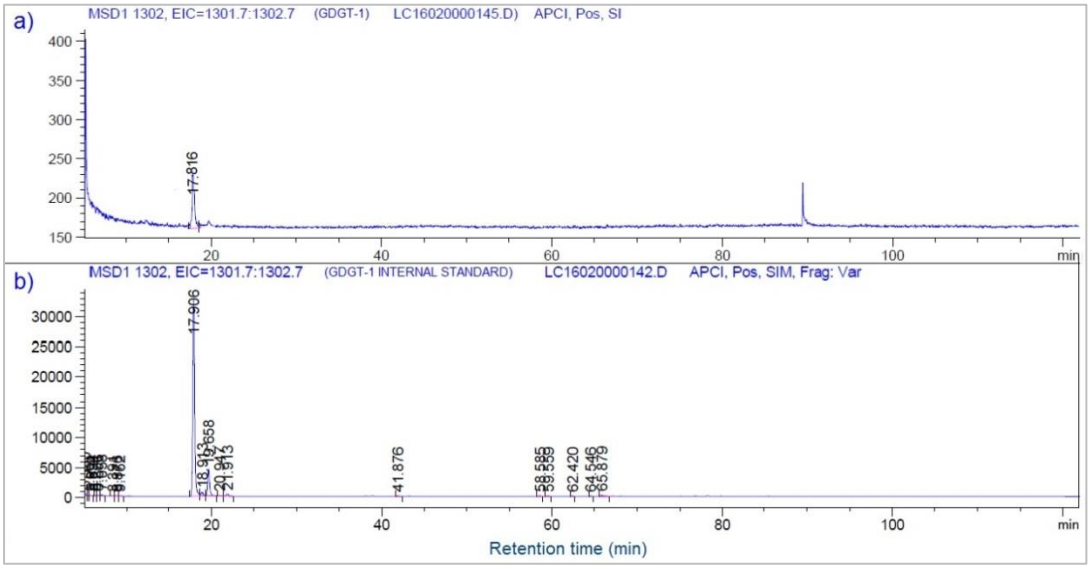

Figure 6: Chromatograms displaying biomolecule **(a)** GDGT-1 peaks of sample N44-2 versus **(b)** GDGT-1 peaks of the used internal laboratory standard. The peaks are set out against the retention time (in minutes). These chromatograms are two examples of the total set of chromatograms presented by the LC-MS.

The chromatograms were studied to determine whether the samples contain sufficient GDGTs and Crenarchaeol for (La)SST reconstructions. Figure 6 compares the concentration of GDGT-1(a) with the used GDGT-1 internal standard (b). As evident from the figure, the peak representing the GDGT-1 of sample N44-2 is significantly smaller and comprises less than 1% of the size of the peak of the in-house standard GDGT-1. The rest of the chromatograms are not shown, notwithstanding the fact that these display similar results of minimal GDGT and Crenarchaeol concentrations.

On account of these minimal biomarker concentrations, it was decided to not apply the proposed temperature proxies TEX_{86} and MBT/CBT for (La)SST reconstructions on the 8 samples of the trial run nor on the other 25 samples. Nonetheless one might argue that even though the values observed in the samples are significantly lower than those of the internal standard, the application of the paleo-thermometer proxies on these biomolecule concentrations may still produce useable results. However earlier empirically gained experience in the field of organic geochemistry strongly suggests otherwise. Although unlikely, a potential limitation of this decision is that by cancelling further organic geochemical analysis, this research missed out on samples that may in fact contain sufficient concentrations for biomarker analysis. Furthermore in view of identifying the reason of the low observed quantities of biomolecules, several possible explanations could be addressed. At first one might argue in favour of degradation of the biomolecules as a consequence of the proposed age of the analysed samples. It is also plausible that the underlying cause might be related to strongly declined abundances of these biomarker producing organisms (extrapolated from, Kim et al.,2008; Peterse et al., 2012).

A possible limitation of the scope of this research is that it did not include alternative methods for reconstructing land or sea surface temperatures, such as the Mg/Ca method (e.g., Anand et al., 2003; Lear et al., 2002), or the $\delta^{18}O$ proxy (on planktic and benthic foraminifera) (e.g., Zachos et al., 1994). Although significant portions of the core interval is barren of calcareous nannofossils (see chapter 2.4). This would support the idea of using cores from another drilling site. This next to the fact that certain taxa of dinocysts that were encountered in the samples of this study could potentially be linked with specific environmental

conditions in terms of temperature. For instance the thriving of dinocyst genera *Apectodinium* and *Hafniasphaera* were associated with minimum SST requirements of 20 and 25°C respectively (Frieling et al., 2016). Yet the at present known temperature affinities of dinocysts are, as is assumed in this research, not accurate enough to reconstruct trends in SST from equatorial regions since most of the studied dinoflagellates species that belong to these dinocysts are extinct. New breakthroughs in this field might have significant implications retrospectively for studies similar to this one in terms of (La)SST.

Lastly it must be noted that since no (La)SST trends are successfully reconstructed in this research, the influence of temperature on paleo-climate and seasonality could not be investigated, hereby restricting the options to put paleo-environmental changes into perspective.

4.2. Age Model and Biostratigraphic Framework

4.2.1. Revising the Age Model

Several of the dinocyst events recorded here in hole 959D are well-calibrated stratigraphically elsewhere: the first occurence [FO] of *Apectodinium spp.* at 851.08 mbsf, *Kallosphaeridium yorubaense* at 872.81 mbsf and *Impagidinium celineae* at 873.85 mbsf, and the last occurrence [LO] of *Alisocysta circumtabulata* at 872.81 mbsf. When related to nannoplankton and planktic foraminifera zonation these events considerably improve the biostratigraphic age model for the Paleocene part of the section (as shown in figure 7 and table 2).

Initially for the age model the 56.0 Ma boundary between the Paleocene and Eocene epoch, or often referred to as the onset of the PETM, was placed at a depth of 804.09 mbsf as proposed by Frieling et al. (2016). Hereafter calcareous nannoplankton zone CP7 was identified in core 44R by Masure et al. (1998) between depths 826.5 and 822.0 mbsf, and was adopted in the model. The age determination of this zone is derived from Gradstein et al. (2012), who set the upper border of CP7 at 57.3 Ma and the lower border at 57.5 Ma. Furthermore both the in the data recorded FO of dinocyst *Apectodinium spp.* as well as the LO of *Alisocysta circumtabulata,* marking respectively the transition from planktic foraminifera [P] merged zones P3b/4 to P2/3a and roughly the start of transition zone P2 to P1c as proposed by Guasti (2005), were adopted as well (see figure 7). In addition to this, Gradstein et al. (2012) put the upper border of the combined P3b/4 zone at the top of zone CP7. Subsequently with the upper border of CP7 and several recorded dinocyst FO and LO established in time, now following Gradstein et al. (2012) again, the upper part of merged P3b/4 zone was dated at 57.3 Ma and the lower border at 61.3 Ma. Moreover since the lower border of P3b/4 was set in time, automatically the upper border of zone P2/3a was also dated hereby (as can be seen in figure 7). Besides this the lower border of zone P2/3a was adopted from Gradstein et al. (2012) as well and placed at 62.6 Ma. Now that multiple points in time were newly identified in the core sections, an age model was calibrated which linearily interpolated these findings, hereby assuming a constant sedimentation rate (as depicted in table 2).

Additionally the in situ recorded FO of dinocysts *Kallosphaeridium yorubaense* and *Impagidinium celineae* (see figure 7) were used to confirm the Danian age following Masure et al. (1998). Nevertheless certain other known first or last occurences of dinocysts from the research of Masure et al. (1998) were excluded from use for age model calibration (e.g. *Palaeocystodinium australinum, Cerodinium diebellii and Tanyosphaeridium xanthiopyxides*). This was done since (crucial parts of) these ranges were based on the identification of a single cyst (as learned from the acquired dataset of dinocyst assemblages), which weakened the confidence of these specific genera in terms of application as a stratigraphic marker considerably (see figure 7). Furthermore the in

Table 2: The configuration of the age model which forms the foundation of the newly proposed biostratigraphic framework. Constant sedimentation rates are assumed between two calibration points, as illustrated. Here light blue rows signify initial calibration points and dark blue rows indicate points added in this study.

Sample id	Age cal. (Ma)	Depth (mbsf)	Sed. rate (Ma/m)	Sed. rate (m/Ma)	Calibration Point
	55,96	**804,09**			1: onset PETM Age
N42-2	56,02	805,12	0,06	16,20	
N42-3	56,10	806,34			
N43-1	56,49	812,72			
N43-2	56,57	813,94			
N43-3	56,67	815,58			
N43-4	56,76	817,08			
N43-5	56,91	819,51			
N43-6	56,99	820,82			
N43-7	57,05	821,77			
N44-1	57,06	821,99			
	57,10	**822,59**			2: FO *D.multiradiatus*
N44-2	57,15	823,04	0,10	9,83	
N44-3	57,26	824,15			
N44-4	57,49	826,45			
	57,5	**826,5**			3: Lower boundary CP7
N44-5	57,63	827,33	0,15	6,47	
N44-6	57,93	829,30			
N44-7	58,14	830,62			
N44-8	58,28	831,53			
N45-1A	58,36	832,06			
N45-1B	58,43	832,55			
N46-1	59,88	841,91			
N46-2A	59,95	842,37			
N46-2B	60,00	842,67			
N47-1A	**61,30**	**851,08**			4: FO *Apectodinium spp.*
N47-1B	61,34	851,73	0,06	17,52	
N48-1	61,87	861,01			
N48-2	61,97	862,79			
N48-3	62,04	864,12			
N48-4	62,13	865,64			
N48-5	62,23	867,40			
N48-6	62,29	868,38			
N49-1	62,41	870,46			
N49-2	62,54	872,805			
N49-3	**62,6**	**873,85**			5: LO *Alisocysta circumtabulata*

the initial age model detailed FO of nannofossil *Discoaster multiradiatus* at 822.59 mbsf, dated at 57.1 Ma (Cleber, 2007; Shafik, Watkins, & Shin, 1998) was used to test the validity of this newly proposed age model (see table 2). The model showed a small inconsistency between this last date and the upper boundary of zone CP7. However because the FO of *D. multiradiatus* was supported by stronger evidence, its age and corresponding depth was adopted In the age model. Furthermore the presence of the K-T boundary at 870.2 mbsf and moreover within the studied interval at all was discarded. This was done due to firstly both typical and stratigraphically significant dinocyst K-T boundary markers *Paleoperidinium pyrophorum* and *Palynodinium grallator* (Evitt, Damassa, & Albert, 1998; Schiøler & Wilson, 1993) were not recorded, secondly it did not agree with the rest of the model, and thirdly the evidence supporting the K-T boundary was meagre (Mascle et al., 1996). Since the here presented analyses do not extent further down to lower cores, the exact position of the K-PG boundary remains elusive.

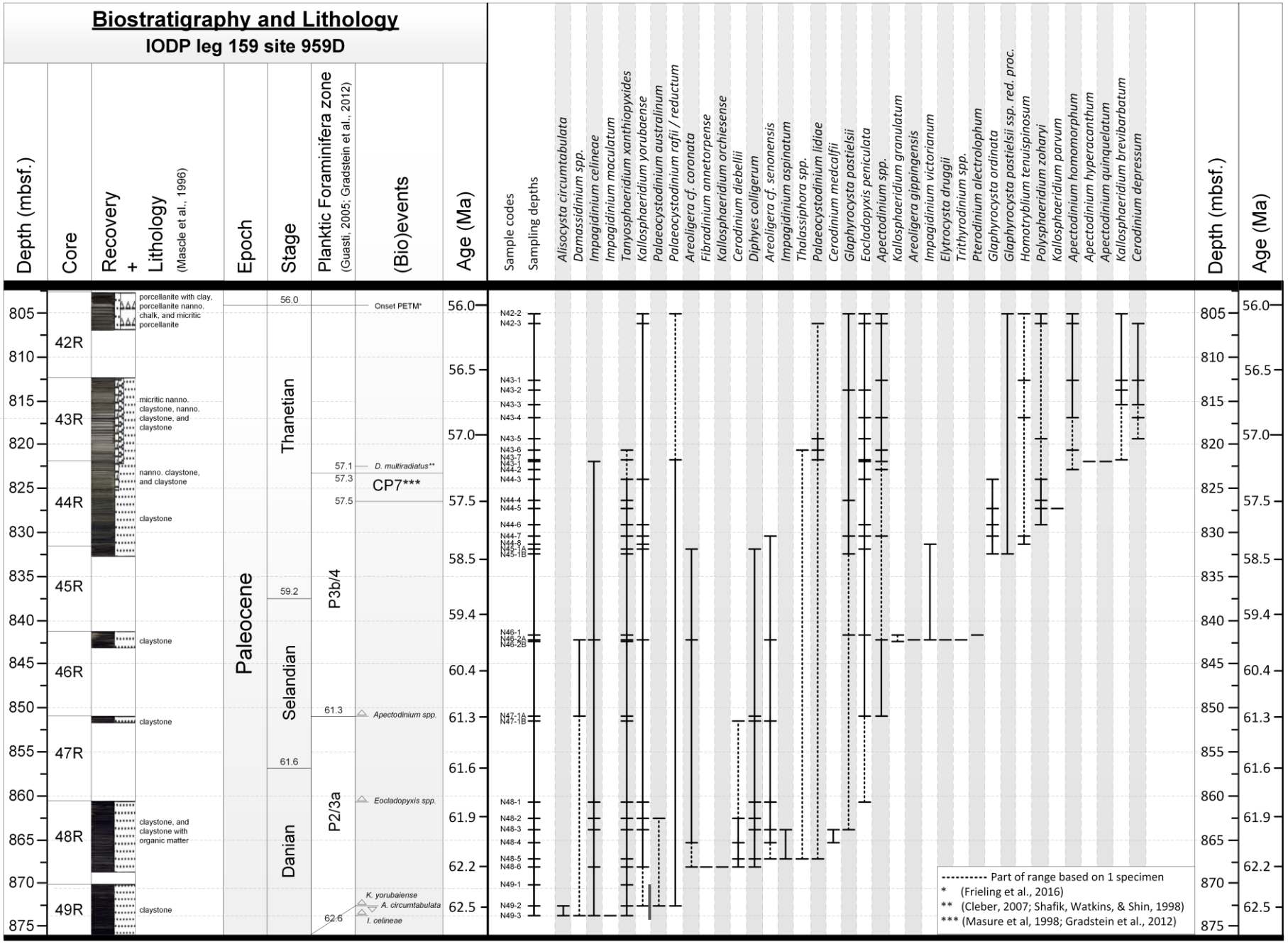

Figure 7: Paleocene ranges of dinocyst taxa, major bio-events, sampling depths, core recovery and the lithology plotted against time and core depth for ODP site 959D. The time aspect and bio-events are based on the age model calibrations as proposed in chapter 2.2.3.2. and include the late Danian, Selandian and Thanetian stages of the Paleocene epoch.

4.2.2. Biostratigraphic Framework Interpretations

As one can learn from figure 7 all three stages of the Paleocene were identified in the investigated core section, yet the Danian appears to be partially captured. In fact the beginning of the Danian is placed at 66.0 Ma (Gradstein et al., 2012), while evidence in the analysed core suggests that only the late part from approximately 62.6 Ma to 61.6 Ma of this stage is captured. Furthermore the 61.6 Ma boundary of the Danian and the Selandian is placed at a core depth of approximately 857.0 mbsf. A few meter up in the drilled cores, the termination of the Selandian and the onset of the Thanetian stage is found at about 837.5 mbsf with a corresponding age of 59.2 Ma. The studied core section fell a little short in capturing the entire Thanetian since the 56.0 Ma Paleocene-Eocene boundary is recorded at a depth of almost 804.0 mbsf, while the upper sample is placed at roughly 805.1 mbsf.

Furthermore the biostratigraphic range chart demonstrates various dinocyst ranges for the tropical Paleocene, that can be related to published research that looked into this as well. Of several of these illustrated dinocysts the first and/or last occurrences have proven to be valuable assets as stratigraphic markers. For instance Crouch et al. (2003) presented the FO of *Homotryblium tenuispinosum* (often referred to as *H. pallidum*) in the Elles section (Tunisia) in the early Thanetian, conform this study's results as shown in figure 7. Other examples that might add to the idea of connecting with near-field studies are given by Masure et al. (1998) and include the LOs of *Cerodinium diebellii* in the Selandian and *Palaeocystodinium australinum* in the Danian stage (see figure 7). Although, as is evident from this figure as well, the upper part of these two dinocyst ranges are based on the identification of a single cyst. This might therefore weaken the confidence of these specific genera in terms of application as a stratigraphic marker in eventual future research.

On the other hand observations of dinocyst ranges from the North-Atlantic and Denmark as presented by respectively Stover et al. (1996) and Heilmann-Clausen (1985), correlate in some cases well (e.g. FO of *Apectodinium homomorphum* at top CP7 zone, and *Glaphyrocysta ordinata* at ~60 Ma). They correspond sometimes weakly (e.g. FO *Apectodinium spp*. at Selandian, and LO *Cerodinium diebellii* at Danian-Selandian). And in other cases they match not at all (e.g. FO *Diphyes colligerum* at Selandian), when related with the newly proposed biostratigraphic model. One may argue that the mismatches from the model can be explained by an inadequate calibration of the revised age model, which was integrated in the proposed biostratigraphic range chart. Yet that does not explain why it does match with studies investigating roughly the same region. Explanations rival to this one include the considerable higher geographical position of these study areas and corresponding diverting paleo-ecosystems and climates, as well as an eventual migration, transport and/or habitat adjusting lag of the mentioned species of dinoflagellates. More specifically in view of paleo-ecosystem and climate, one may hypothesise that it might take a while before the environmental conditions at higher latitudes match the tolerances of dinoflagellates or vice versa in periods of climate change. Whereas dinoflagellate migration, transport and/or habitat expansion is mainly subject to ocean currents (Garrison, 2013). Evidently it may also take some time before ocean currents that can sustain certain genera of dinoflagellates to some extent, transport sufficient quantities to start a new population fast enough, and the setting where it flows to/along is habitable. It is hypothesised here that these are all crucial factors which are required to co-occur in order to facilitate a successful migration, and thus will most likely results in lag. Subsequently the scope of this research lies elsewhere, hence no further details about the underlying mechanisms will be discussed.

Apart from that roughly the same order of conformity and deviation is observed when comparing the results of the biostratigraphic study performed by Brinkhuis, et al. (2003), who studied ODP site 1172 located near the south-east coast of Australia. Although this site is situated at approximately the same latitude, the absolute spacing between ODP site 1172 and the here studied ODP site 959, is large on a global scale. Again the

observed deviations may therefore be explained by diverting paleo-ecosystems, an inaccurate age model and/or migration lags, and less so by dissimilar paleo-climates.

Ultimately the previously discussed and other unmentioned dinocysts that are shown in the newly proposed biostratigraphic framework might be used to confirm and/or relate the findings of both published and future research that investigate the tropical Paleocene and adjacent epochs biostratigraphically. However considering the earlier discussed relations of this study with research that investigated Paleocene dinocyst assemblages originating from the near field, distant regions, or middle to high latitudes for that matter, gives ground to the belief that the use of the proposed framework is most trustworthy when applied on a regional basis (i.e. sites in proximity of 959D).

4.3. Paleocene Paleo-environmental Reconstructions

The palynomorph assemblages used for the paleo-environmental reconstructions consist predominantly of dinoflagellate cysts, which typically fluctuates around 75% of the relative total (see figure 8l). Whereas absolute dinocyst values can reach up to roughly 12,000 per gram sample (as depicted in figure 9). A distinct acritarch peak (40-60%) is recorded in the upper section between 821.99 and 819.51 mbsf though (fig. 8l). When sorted, the three most dominant taxa/groups of dinocysts observed in the samples are *Spiniferites spp*. (21-95%), *Operculodinium spp*. (2-47%) and *Areoligera cpx.* (0-47%) as demonstrated in figure 8.

In order to present the aimed paleo-environment reconstruction of the Paleocene, interpretations were done in terms of paleo-oceanological settings, paleo-productivity and past sea level fluctuations. Hereby following the palynological implications as proposed in chapter 3.1.4 and those related to the geological setting as detailed in chapter 2.2.

4.3.1. Paleo-oceanological Settings

In general the *Operculodinium spp.* abundances (10-50%) found in the late Danian (862.69 mbsf) to early Thanetian (829.30 mbsf) suggest episodes where open marine settings prevailed, and the continuous contemporary presences of *Impagidinium spp.* even point towards open ocean conditions (see figure 8). Elevated levels of the *Operculodinium* genus are also known to indicate a signal of enhanced transport. As detailed before free flowing equatorial surface waters were suspected in the Deep Ivorian Basin of the Paleocene (Wagner, 2002) and could transport dinoflagellates over long distances (Garrison, 2013). In theory enhanced oceanward surface currents could have increased the likelihood of dinocysts of the African shelf to reach site 959 and be deposited there. Contemporary rises in the inner neritic favouring *Areoligera* complex [cpx.] (fig. 8b) as well as the lagoonal *Senegalinium* group (fig. 8g) provides supporting evidence for this. Furthermore coastal surface waters are often influenced by (seasonal) fluvial run-off, which provides an input of pollen and spores to these waters although they are also subject to aeolian transport (Garrison, 2013). In the late Danian through early Thanetian pollen and spores consist between 5-20% of the total palynomorphs (see figure 8l). The presumed paleo-location of site 959 at ~4.5°S near the southwest African coast and within the ITCZ (figure 3) (PALEOMAP Project, 2000) would enable sufficient fresh water input to fluvial systems through seasonal monsoonal precipitation (Garrison, 2013), which could end up in the African shelf ocean. Furthermore the increases of the brackish water indicator *C. fibrospinosum* group (fig. 8c) match to some extent those seen in *Operculodinium* (fig. 8f) timewise. When related with the moderately frequent pollen and spores observations, one may interpret this as additional support of coastal waters reaching site 959 through strengthened surface currents. Yet local conditions at the Transform Margin could also have influenced the here presented signals.

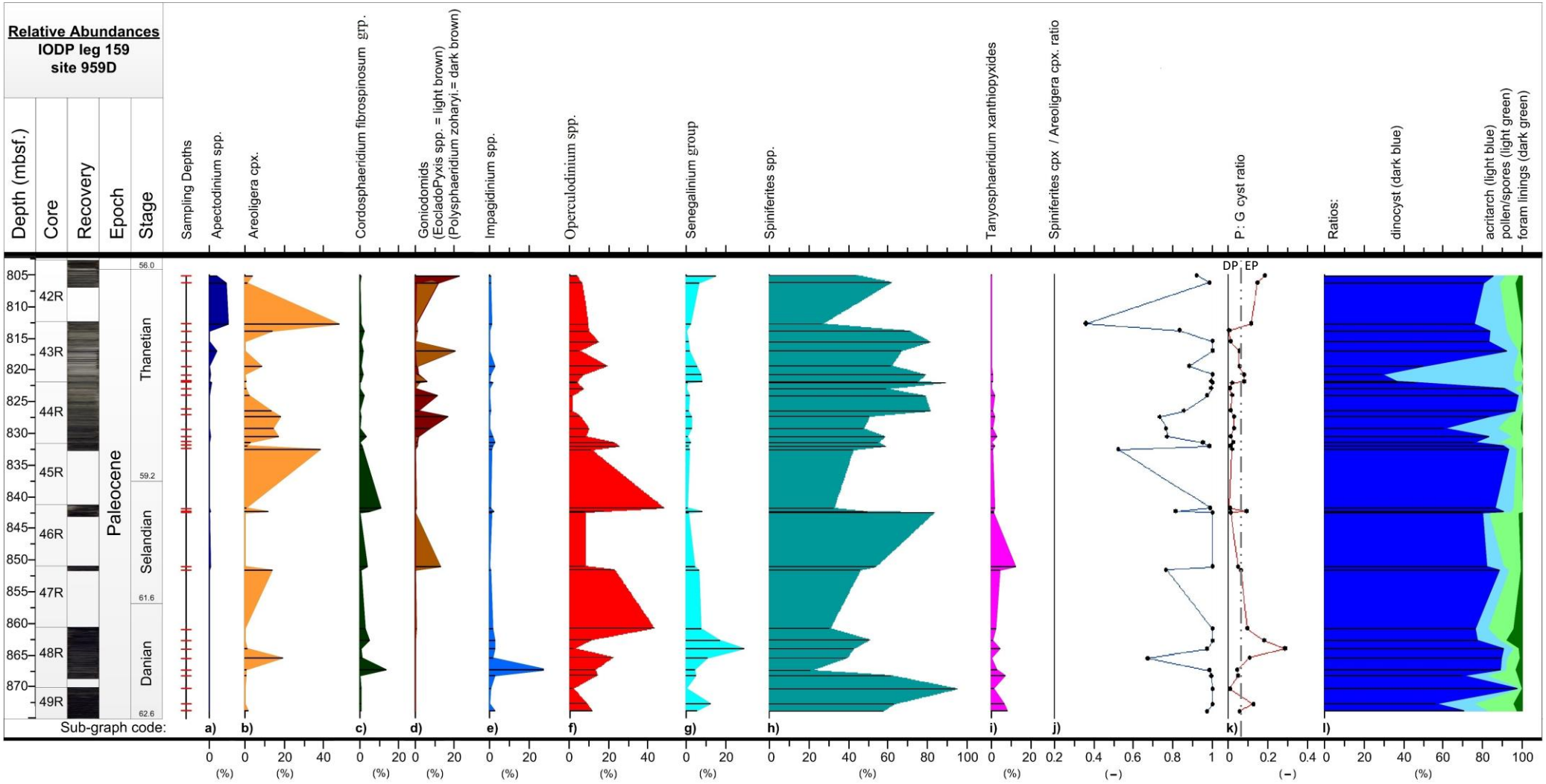

Figure 8: The early to latest Paleocene as recorded by multiple palynological proxies based on dinocysts and palynomorphs, core photographs, core depth and sampling intervals for ODP site 959D. Hereby the grouping as proposed by Guasti (2005) and Sluijs & Brinkhuis (2009) was followed. Subgraphs **(a) to (i)** reflect for several dinocyst taxa the relative abundance in percentage of total dinocysts. Subfigure **(j)** and **(k)** display respectively the Spiniferites : Areoligera cpx. ratio and the P:G cyst ratio, in these two graphs the dotted lines represent the mean value of the ratios. The mean values were added to subfigure (i) to signify outer neritic (ON) and inner neritic (IN) settings**,** whereas to subfigure (j) to point out elevated levels of marine primary productivity (EP) levels and decreased primary productivity (DP). **(l)** Ratio total dinocyst (dark blue), acritarchs (light blue), pollen and spores (light green), and foram linings (dark green) in percentage of the total sum of these four palynomorph groups.

Furthermore peak abundances in specimens of the Goniodomid group (up to 22%) are predominantly found in the middle to late Thanetian interval (figure 8c), and are related to lagoon-like, as well as hypo-/hypersaline, conditions. These increases co-occur with decreases of *Operculodinium* and may be interpreted as periods of more restricted marine conditions in the proximity of site 959. Nevertheless the continuing presence of *Impagidinium* tends to point towards ongoing open ocean influences, which would imply that the Goniodomid abundances may in fact reflect a signal of transport.

4.3.2. Paleo-productivity

Substantial (above-average) P-cyst increases are recorded at both ends of the core which are aged as late Danian and middle to late Thanetian (figure 8k), as well as a brief rise at 842.37 mbsf in the late Selandian, that suggest enhanced paleo-productivity. These intervals seem to coincide with enhanced absolute dinocyst and foraminifera abundances (see figure 9), which can be related to elevated productivity as well. As is evident from figure 8g contemporary peaks in the *Senegalinium* group are also found here. The latter group usually indicates nutrient rich concentrations and/or low salinity in the water column, which could have fuelled paleo-productivity in the Deep Ivorian Basin. The origin of these nutrients could be terrestrial that enriched the water column of the shelf ocean through rivers (Ruddiman, 2014). The rise in pollen and spores observed at 872.81 mbsf for instance would emphasize towards this. Although these can reach the site through wind dispersal as well (Ruddiman, 2014). Nevertheless at certain core-depths pollen and spores are scarce, while *Senegalinium* and the P-G ratio point toward respectively high nutrient concentrations and paleo-productivity (e.g. at 864.12 mbsf, figure 8). Here another explanation would deem more plausible. As detailed in chapter 2.2, evidence of nutrient rich deep water, wind-induced upwelling, free flowing surface currents, transport of organic matter and an OMZ near site 959 was found for (parts of) the Paleocene. Hypothetically (seasonal) upwelling of nutrient-enriched deep water could fuel paleo-productivity in coastal waters (Ruddiman, 2014), such as at the African shelf, Deep Ivorian Basin and Transform Margin. Since the deposition of sediments and organic matter at site 959 was most likely a combined signal of transport of the African continental shelf and a local signal (Frieling et al., 2016), organic matter and nutrient abundances could have been transported to site 959 through oceanward equatorial surface currents. Whereas the eventual presence of a significant OMZ surrounding site 959 would have enhanced preservation of organic matter due to a general lack of oxygen to drive degradation. The OMZ may then be sustained due to an abundant input of organic matter. Stratification would have resulted in sharply declined upwelling of nutrients, but could also support a significant OMZ (Garrison, 2013). Spikes in the *C. fibrospinosum* group or the Goniodomid *Polysphaeridium zoharyi* in the Thanetian imply such (hyper-)stratified conditions in the surface water column (see figure 8). The suspected water depth at site 959 was bathyal to abyssal (Oboh-Ikuenobe, 1997), which could host the establishment of a substantial OMZ. Additionally the studied core sections did not demonstrate any significant proof of reworking, since hardly any dinocyst specimen suspected of being reworked is recovered (data not included). This might imply weak bioturbation in the investigated cores that can be explained by bottom anoxia for instance and could indicate an significant OMZ in the water column. A limitation in this assumption is that scarce signs of reworking do not necessarily rule out bioturbation entirely.

Furthermore the peak abundances of *Spiniferites* (>80%) seem to correlate with low productivity (P-G ratio) and reduced nutrient availability in water column (*Senegalinium*) (e.g., 870.46 mbsf, fig. 8). This might be explained by the fact that *Spiniferites* is considered to be an autotrophic generalist taxon (Brinkhuis, 1994), and could thus thrive where other dinocyst taxa were (more) limited by environmental factors (as demonstrated in figure 8).

When comparing the colour alternations of the core photographs with the P-G ratio (figure 8), these proxies appear to be both related towards organic rich environments. However the use of these photographs as an additional palynological proxy to identify organic rich environments was used with reserve, since dark core material, according to Mascle et al. (1996), is *likely* to indicate organic rich paleo-environments. Moreover this

statement also insinuates, that the dark discoloration may as well have had an alternative unmentioned cause, such as diagenesis or substantial preservation related to anoxic conditions for instance.

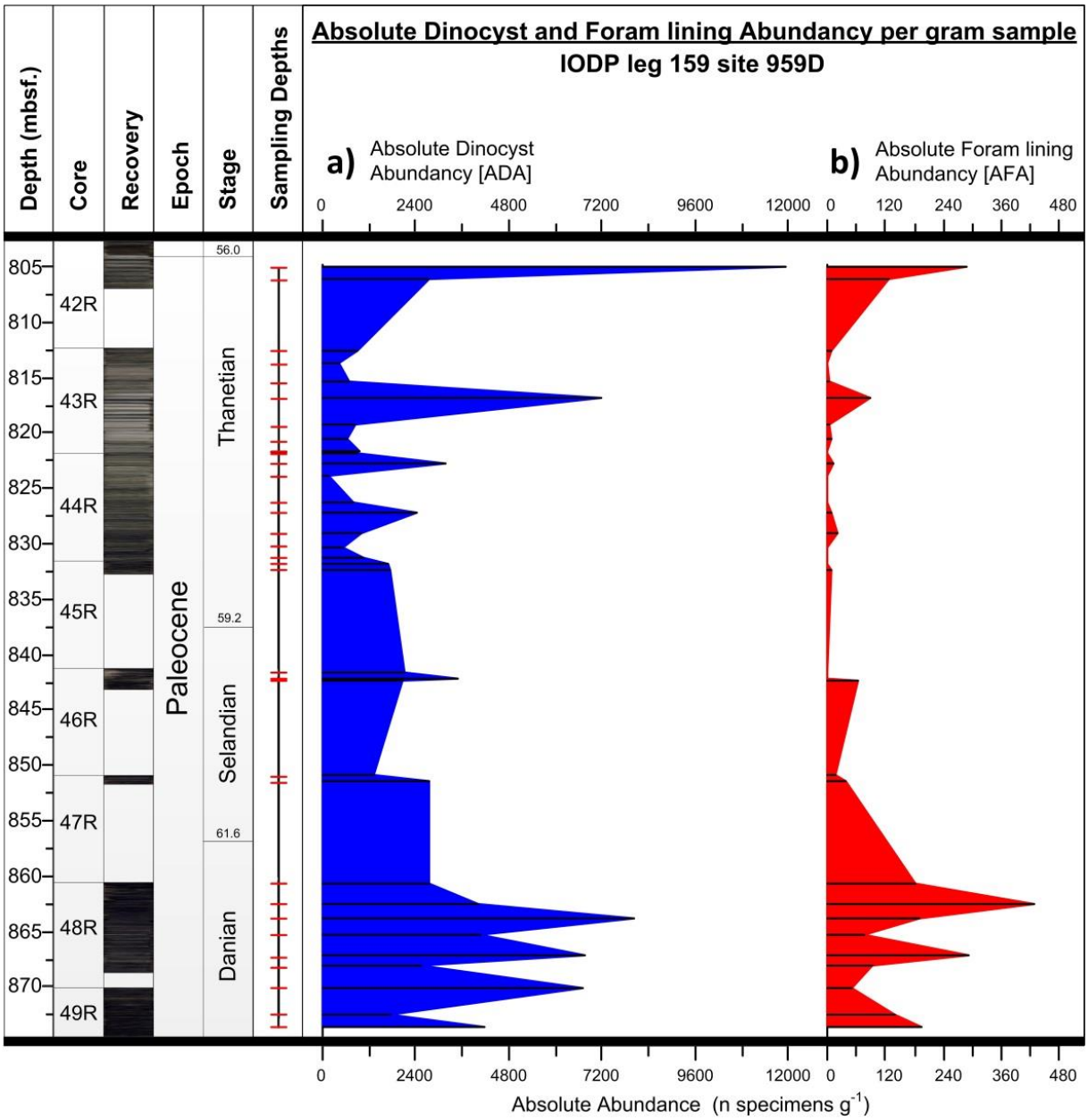

Figure 9: Absolute abundances of (a) total dinocysts and (b) foram linings, sampling depths and core photographs for ODP site 959D in the early to latest Paleocene. The absolute abundances are denoted in number of specimens per gram sample-sediment.

4.3.3. Past Sea Level Fluctuations

In view of investigating the presence of Paleocene continental ice-sheets, one of the stated aims, the S:A ratio was analysed since it is linked with local sea level change (Sluijs et al., 2005). Moreover it is theorised that these local sea level variations can be potentially interpreted to represent global eustatic sea level fluctuations as well (Sluijs et al., 2008). When interpreting the ratio following Sluijs et al. (2005) it shows considerable variability which may suggest transgression or regression events. Long-term trends are not observed in the S:A ratio though.

As illustrated in figure 8j the sharpest shifts from outer neritic towards inner neritic values that could indicate regression are recorded in the late Danian between 867.40 – 865.64 mbsf (~62.1 Ma), the middle-late Thanetian

at 815.58 to 812.72 mbsf (± 56.5-56.8 Ma) and possibly in the earliest Thanetian (ca. 58.5 Ma). Although a considerable hiatus in the core retrieval is found in the latter period, which masks an eventual (regressive) build-up prior to this *Areoligera* dominance of 0.45 at 832.55 mbsf (see figure 8j). In theory these shifts in the S:A ratio might partly be ascribed to sea level fall (Sluijs et al., 2005) and thus an eventual substantial loss of ocean water due to significant accumulation of continental ice volume. One might therefore argue in favour of possible ice sheets in the above mentioned periods (i.e. ± 62.1, 58.5, 56.5-56.8 Ma). When comparing these specific situations with a comparable study performed by Guasti (2005), similar results can be found. More specifically Guasti (2005) also proposed declined sea levels around 58.5 and 56.5-56.8 Ma in North-West Tunisia, which might add to the reliability of some of the results. Additionally when comparing the proposed dates of suspected ice sheets with the high resolution isotope records for the Paleocene of Westerhold et al. (2011), the late Danian and Thanetian ages seem to correspond with intervals of (minor) positive benthic foraminifera $\delta^{18}O$ excursions (~ +1 ‰). It is known that $\delta^{18}O$ values can reflect a combination of deep-sea temperature changes and, if present, changes in ice volume. Moreover it may imply that the $\delta^{18}O$ isotope, as detailed by Westerhold et al. (2011), could thus (partly) reflect changes in ice volume for this time interval. The positive $\delta^{18}O$ excursions are somewhat minor though, which may preclude the possibility of major ice sheet installation during the Paleocene epoch. Since correlations between this study's results and those of Westerhold et al. (2011) and Guasti (2005) were observed, one might argue that the presence of continental ice sheets in the (mid-)Paleocene period for one cannot be excluded.

Furthermore the most notable transitions from inner neritic to outer neritic values can be observed in the late Danian between 865.64 – 864.12 mbsf (~62.0 Ma), early Thanetian from 832.55 to 832.06 mbsf (around 58.2 Ma) and late Thanetian at 812.72 – 806.34 mbsf (ca. 56.3 Ma) interval. In terms of continental ice sheets, these transitions may to some extent be ascribed to a significant loss in glacial volume, which in turn led to a significant (fresh) water input into the ocean. This would have resulted in global elevated sea levels and thus possibly transgression events at site 959. However, apart from the late Thanetian (at ~56.3 Ma), similar trends are not clear from the by Westerhold et al. (2011) recorded $\delta^{18}O$ isotope signals. As shown in figure 8a, the first abundant presence of *Apectodinium spp*. (~10%) is also demonstrated in the late Thanetian. Its first abundant presence is generally well correlated with the late Paleocene at equatorial latitudes. To be specific Crouch et al. (2003) presented comparable results in a study of the Tunisian region, Guasti (2005) showed the same in Egypt and Frieling et al. (2016) demonstrated similar, but more pronounced, trends in Nigeria and Ivory Coast (i.e. site 959) as well. Moreover these first abundant presences in *Apectodinium* have been linked with periods of global climatic warming (e.g., Sluijs & Brinkhuis, 2009) and thus might possibly connected to ice volume loss. However other factors might also explain the increases in *Apectodinium*, including low salinity, elevated sea-surface temperature and nutrients availability (Sluijs et al., 2005). One could only speculate to the forcing behind eventual relative rapid losses in continental ice sheet volume, apart from the fact that it is most likely climate related. Although strong positive feedbacks (e.g. the Albedo feedback) are related to a relatively fast decline in ice sheet volume as well (Ruddiman, 2014).

Nevertheless the by the S:A ratio suggested regression and transgression events cannot be adopted one to one. At site 959 the *Areoligera* and *Spiniferites complex* signals (see resp. figure 8b & 8h) were most likely influenced by transport of the African continental shelf as well as local conditions at the Transform Margin. The S:A ratio proxy was developed for use on a wide stable continental shelf environment (Sluijs et al., 2008). However the geological setting at site 959 is notably deviating from such a continental shelf (Frieling et al., 2016) since the setting was predominantly open marine to pelagic at the Transform Margin, as detailed by Wagner (2002) and discussed in chapter 4.3.1. This means that water depth and shore proximity proportionally change dissimilarly as may be expected from sites on which the S:A ratio is based. Apart from the local signal which is thus difficult to relate to sea level change (Frieling et al., 2016), it can be argued that transport of material from the African

continental shelf through seaward surface currents (as also stressed out in 4.3.1) would still more or less preserve the shelf ratio between both dinocyst complexes. This due to the fact that the wide African continental shelf does match the setting on which the S:A ratio is based. Moreover a suggestion is that at lowered sea levels the likelihood increases of inner neritic dinocysts (e.g. *Areoligera*) being transported more easily from this shelf towards site 959 due to reduced absolute distances. The previous arguments insinuate that sea level shifts could to some extent be imprinted in the recorded S:A ratio signal. It must be noted though that seaward transported neritic cysts in surface currents are subject to several factors which may influence taxa distributions in the recorded sediments (Wall et al, 1977). According to Wall et al. (1977) these factors include terrestrial run-off, outwash from lagoons, coastal upwelling and mixing of different water masses.

Additionally if the by the S:A ratio recorded eustatic sea level variations are indeed to some extent imprinted, it is probably a combined signal which is comprised of several far- and near-field factors that each have some degree of influence on global sea level. The main factors include tectonic activity, steric effects and ice sheet volume (e.g., Sluijs et al., 2008). Firstly the Paleocene was indeed subject to significant tectonic processes. For instance the North Atlantic Igneous Province [NAIP], which was a significant magmatic active region in the North Atlantic, was most active between 60.5 and 54.5 Ma based on isotopic dating (Jolley & Bell, 2002). During this active phase large amounts of young oceanic crust was produced, which most likely elevated parts of the ocean floor and resulted in global eustatic sea level rise to some extent (Sluijs et al., 2008). This coincides with a substantial part of the recorded time interval of this research which ranges from roughly 62.6 Ma (late Danian) to 56.1 Ma (late Thanetian just before the onset of the PETM), as proposed in this study. Furthermore the investigated site 959 lays on a tectonically active basin (Mascle et al., 1996), which is why subsidence or uplift of the studied site cannot be excluded as a contributing factor as well. Another main factor is the steric effect, which refers to the thermal expansion of the ocean water under influence of temperature forcing. This could potentially be related to (La)SST trends of the tropical Paleocene. Regrettably, as outlined in paragraph 4.1, these (La)SST could not be reconstructed in this research and thus limits the options to look into its relative influence. On the other hand the influence of steric effects at other regions in the Atlantic Ocean can be investigated for the Paleocene. Sluijs et al. (2008) for instance concluded that the steric effects were not a dominant contributing factor in long-term sea level (i.e. in periods ≥ 100 kiloyears) in (mid-latitude) New Jersey for the late Paleocene (Thanetian), prior to the onset of the PETM. Whereas Frieling et al. (2016) displayed contemporary long term sea surface temperature [SST] shifts of ~1.5°C based on TEX_{86} in Nigeria. Apparently temperature shifts in this order of magnitude at these latitudes did not contribute dominantly in long-term sea level change. Frieling et al. (2016) also reconstructed SST trends for parts of the Selandian stage. However it is uncertain to what extent the Selandian is captured within their records. Yet more importantly in this suspected Selandian interval, no SST change greater than 1.5 °C is recorded. In addition to this Westerhold et al. (2011) suggested that the mid-Paleocene (Selandian to Thanetian) was in a climate minimum state, with potential greenhouse gas values and possibly ice sheets comparable to modern times. This would imply that the steric effects could be ruled out as a major contributor to reflect long-term sea level fluctuations in the Selandian (partly) and Thanetian stages. Lastly the remaining important contributing factor is changes in polar ice volume. Strong evidence that could point towards major continental ice sheets is lacking though.

5. Conclusions

This research enabled studying the aimed paleo-environmental changes and an improvement of the biostratigraphic framework of the equatorial Paleocene by means of applying palynological proxies on recorded dinocyst assemblages acquired from ODP site 959, offshore Ivory Coast (west-Africa).

No clear patterns were recognised in the evolution of the suggested Paleocene paleo-environments towards the onset of the PETM at site 959. Furthermore interpretations of the dinocyst assemblages suggest a prevailing open marine to even pelagic setting here, which is implied by Wagner (2002) as well. The assemblages also imply that paleo-productivity at site 959 was probably controlled by wind-induced upwelling of nutrient rich deep water and fluvial input of nutrients, as well as (seasonal) stratification and sea level fluctuations. Unfortunately no land and sea surface paleo-temperatures were reconstructed, due to insufficient biomarker concentrations in the studied samples. As a consequence the insights in the distribution of heat and its forcing on climate change during the equatorial Paleocene remain limited, in the context of mid-Paleocene greenhouse and its transition towards Eocene “hothouse” conditions.

Furthermore the in the presented data recorded first occurrence of *Apectodinium spp.*, *Kallosphaeridium yorubaense* and *Impagidinium celineae*, and the last occurrence of *Alisocysta circumtabulata,* were related to nannoplankton and planktic foraminifera zonation and improved the existing biostratigraphic age model for the Paleocene. Comparison of the proposed biostratigraphic framework with related contemporary frameworks detailing near field and distant regions, gave ground to the belief that the use of the proposed framework is most trustworthy when applied on a regional basis.

In light of continental ice sheets, the most plausible presences were suspected for mid to late Paleocene ages (~62.1-56.3 Ma) on ground of the S:A ratio results of this study and the findings of Crouch et al. (2013), Guasti (2005), Frieling et al. (2016) and Westerhold et al. (2011). Yet direct and strong evidence for prominent ice sheets is lacking. The reliability of the S:A ratio to reflect sea level changes is also questionable, since firstly it was developed for use on a different depositional setting and secondly it likely reflects both a local and a transported signal. This next to the fact that even if the S:A ratio indeed recorded eustatic sea level variations, the latter was probably a combined signal of tectonic activity, steric effects and ice sheet volume. It remains therefore unclear whether the $\delta^{18}O$ isotope trends, as detailed by Westerhold et al. (2011), reflect substantial fluctuations in polar ice volume or predominantly a temperature signal for the equatorial Paleocene.

Acknowledgements

Before the ink runs out I would like to express my appreciation and gratitude to a number of people who supported me in my "MSc thesis quest".

First of all I would like to thank my thesis supervisors Peter Bijl and Appy Sluijs, as well as my partners in crime and members of the 959-fellowship Joost Frieling and Margot Cramwinckel, who took me under their metaphorical wings and whose guidance, assistance and investment of their precious (no, no ring here Gollum) time proved inspirational and more importantly vital.

I am also grateful towards the people of the GML laboratory, who safely and sensibly guided this loose cannon through an environment completely filled with unhealthy substances, and even enabled me to leave the lab unscathed time after time. Thank you for that Natasja and Dominika.

Furthermore I would like to say thank you to my *brothers and sisters in arms* of the fifth floor studentsroom. Ilja, Emiel, Pam, Michelle, Wilrieke, Jorieke, Christine, Hans, Koen, Anja, Nikki, Machteld, and the rest, you made me laugh all the time, gave me often much needed distractions through "tablesoccer" or "De Speld" updates , looked out after me and each other, respected my territorial drift, huge mess and music addiction, helped me out in dire need and thus, long story short, made sure that I had a really good time while doing my thesis research in Utrecht. So as promised in the beginning of this piece of text, to you I say: thank you.

Also I would like to salute to Eldin Honingh for the frequent, fun and much needed coffee breaks.

Besides this all those people who remain unmentioned, but nevertheless played an undoubtedly crucial role in the help-mike-finish-his-thesis muppet show, thank you.

Last of all special thanks to my parents Sytse and Mirjam, and of course to my two brothers Roy and Mitchell, for their unconditional support and, when required, understanding of alone time during my "cave-phase".

Mike

Appendices

A: Abbreviations
B: Encountered Dinoflagellate Species List
C: Unknown Dinoflagellate Cysts and Palynomorphs
D: Dinocyst Plates
E: Statement of originality of the MSc thesis

Appendix A: Abbreviations

Acronym	Definition
ADA	Absolute Dinocyst Abundancy
AFA	Absolute fossilised organic benthic Foraminifera linings Abundance
ASE 350	Accelerated Solvent Extractor type 350
mbsf	meters below sea surface
CP zone	Calcareous nannoPlankton zone
DCM	DiChloroMethane
FO	First Occurrence
G cyst	Gonyaulacoid cyst (i.e. tabulation type)
GDGT	Glycerol Dialkyl Glycerol Tetraethers
HCL	HydroChloric acid
HF	HydroFluoric acid
ITCZ	InterTropical Convergence Zone
K-T boundary	Cretaceous-Tertiary boundary
ky	kilo year or 1000 year
Ma	Mega annum / Million years ago
NAIP	North Atlantic Igneous Province
ODP	Ocean Drilling Program
(La)SST	(Land and) Sea Surface Temperatures
LC-MS	Liquid Chromatography–Mass Spectrometer
LO	Last Occurrence
MeOH	Methanol
ODP	Ocean Drilling Program
P zone	Planktic foraminifera zone
P cyst	Peridinioid cyst (i.e. tabulation type)
PETM	Paleocene-Eocene Thermal Maximum
pp	primary productivity
S:A ratio	Spiniferites : Areoligera ratio
sf	subfigure
SSP	Sea Surface Productivity
SST	Sea Surface Temperature

Appendix B: Encountered Dinoflagellate Species List

Gonyaulacoid cyst	References	Remarks	In document
Achomasphaera crassipellis	(Stover & Evitt, 1978)		
Adnatosphaeridium multispinosum	(Williams & Downie, 1966)		Plate 1B
Alisocysta circumtabulata	(Stover & Evitt, 1978)		Plate 1A
Areoligera cf. coronata	(Du Chêne & Adediran, 1984)		Plate 1D
Areoligera gippingensis	(Jolley, 1992)		Plate 1E &1F
Areoligera cf. senonensis	(Du Chêne & Adediran, 1984)		Plate 2A
Areoligera senonensis	(Lejeune-Carpentier, 1938) emend. Lejeune-Carpentier & Sarjeant, 1981		
cf. Batiacasphaera sp. A		Unclassified , but resembles a species of the genus *Batiacasphaera*, detailed in Appendix C	Appendix C
cf. Batiacasphaera sp. B		Unclassified, but resembles a species of the genus *Batiacasphaera* detailed in Appendix C	Appendix C
Cordosphaeridium fibrospinosum	(Davey & Williams, 1966) emend. Davey, 1969b		
Cordosphaeridium multispinosum	(Davey & Williams, 1966)		
Cribroperidinium sp. A		J. Frieling uses the same nomenclature for this cyst type	
Diphyes colligerum	(Deflandre & Cookson, 1955) emend. Cookson, 1965; emend. Davey & Williams, 1966; emend. Goodman & Witmer, 1985		Plate 2E
Damassadinium sp.		Species not recognised	Plate 2D
Dapsilidinium sp.		Species not recognised	Plate 2F
Elytrocysta druggii	(Stover & Evitt, 1978)		Plate 3A
Eocladopyxis peniculata	(Morgenroth, 1966) emend. McLean, 1976		Plate 3B
Florentinia reichartii	(Sluijs et al., 2009)		Plate 3C
Florentinia ferox	(Deflandre, 1937) Duxbury, 1980		
Fibradinium annetorpense	(Morgenroth, 1968)		Plate 3D
Fibrocysta axialis	(Eisenack, 1965) Stover & Evitt, 1978		
Fibrocysta bipolaris	(Cookson & Eisenack, 1965) Stover & Evitt, 1978		
Fibrocysta. cf. lapacea	(Du Chêne & Adediran, 1984)		
Glaphyrocysta ordinata	(Williams & Downie, 1966) Stover & Evitt, 1978		
Glaphyrocysta pastielsii	(Deflandre & Cookson, 1955) Stover & Evitt, 1978; emend. Sarjeant, 1986		
Glaphyrocysta pastielsii ssp. reduced processes		Unclassified, potential new subspecies of G*laphyrocysta pastielsii*, detailed in Appendix C	Appendix C
Hafniasphaera septata	(Cookson & Eisenack, 1965) Hansen, 1977		Plate 3E
Homotryblium tenuispinosum	(Davey & Williams, 1966)		
Hystrichokolpoma rigaudiae	(Deflandre & Cookson, 1955)		Plate 3F
Impagidinium aspinatum	(Cookson & Eisenack, 1974) Damassa, 1979		Plate 4C
Impagidinium celineae	(Du Chêne & Adediran, 1984)		Plate 4A & 4B
Impagidinium maculatum	(Cookson & Eisenack, 1961) Stover & Evitt, 1978		Plate 4D
Impagidinium parvireticulatum	(Wilson, 1988)		

Impagidinium victorianum	(Cookson & Eisenack, 1965) Stover & Evitt, 1978		Plate 4E
Kallosphaeridium brevibarbatum	(De Coninck, 1969) emend. Du Chêne, Stover & De Coninck,1985		Plate 4F
Kallosphaeridium granulatum	(Norvick & Burger, 1976) Stover & Evitt, 1978		Plate 5A
Kallosphaeridium orchiesense	(De Coninck, 1975) emend. Du Chêne et al., 1985		Plate 5C
Kallosphaeridium parvum	(Jan R. Du Chêne, 1988)		
Kallosphaeridium yorubaense	(Du Chêne & Adediran, 1984)		Plate 5B
cf. Melitasphaeridium pseudorecurvatum	(Deflandre & Cookson, 1955) Wall, 1967	Unclassified , but resembles a species of the genus *Melitasphaeridium*, detailed in Appendix C	Appendix C
Operculodinium centrocarpum			
Operculodinium? cf. fibrocysta		*Unclassified , but resembles the genera Operculodinium and Fibrocysta, detailed in* Appendix C	Appendix C
Polysphaeridium zoharyi	(Rossignol, 1962) Bujak et al., 1980a		Plate 6E
Pterodinium alectrolophum	(Sarjeant, 1966) Below, 1982		Plate 6D
Pyxidiniopsis ardonensis	(Du Chêne, 1988)		
Spiniferites? cf. celineae		Unclassified , but resembles *Spiniferites* and *Impagidinium celineae*, detailed in Appendix C	Appendix C
Spiniferites mirabilis	(Rossignol, 1964) Sarjeant, 1970		
Spiniferites pseudofurcatus	(Klumpp, 1953) Sarjeant, 1970; *emend.* Sarjeant, 1981		
Spiniferites pseudofurcatus ssp. granulosum	(Schiøler, 1993)		
Tanyosphaeridium xanthiopyxides	(Wetzel, 1933*;* emend. Morgenroth, 1968*)* Stover and Evitt, 1978; emend. Sarjeant, 1985		Plate 7A
Thalassiphora pelagica	(Eisenack, 1954) Eisenack & Gocht, 1960*;* emend. Benedek & Gocht, 1981		
Trichodinium sp.	(Du Chêne & Adediran, 1984)		Plate 7B
Peridinioid Cysts	**References**	**Remarks**	**In document**
Apectodinium homomorphum	(Deflandre and Cookson, 1955) Lentin & Williams, 1977		
Apectodinium hyperacanthum	(Cookson and Eisenack, 1965) Lentin and Williams, 1977		Plate 1C
Apectodinium quinquelatum	(Williams and Downie, 1966) Costa & Downie, 1979		
Cerodinium depressum	(Morgenroth, 1966) Lentin and Williams, 1987		
Cerodinium diebellii	(Du Chêne & Adediran, 1984)		Plate 2C
Cerodinium leptoderma	(Du Chêne & Adediran, 1984)		
Cerodinium medcalfii	(Stover, 1974) Lentin and Williams, 1987		Plate 2B
Lejeunecysta fallax	(Morgenroth, 1966) Artzner & Dörhöfer, 1978*;* emend. Biffi & Grignani, 1983		
Palaeocystodinium australinum	(Cookson, 1965b*;* emend. Malloy, 1972)		Plate 5E

	Lentin & Williams, 1976		
Palaeocystodinium golzowense	(Alberti, 1961)		Plate 5D
Palaeocystodinium lidiae	(Gorka, 1963) emend. Davey, 1969		Plate 6A
Palaeocystodinium rafii/ reductum	(May, 1980)		Plate 6B
Phelodinium magnificum	(Stanley, 1965) Stover and Evitt, 1978		
Phelodinium sp.		Species not recognised	Plate 6C
Phtanoperidinium crenulatum	(De Coninck, 1975) Lentin and Williams, 1977; emend. Heilmann-Clausen, 1985		
Senegalinium microgranulatum	(Stanley, 1965) Stover and Evitt, 1978		
Senegalinium obscurum	(Drugg, 1967) Stover and Evitt, 1978		

Appendix C: Unknown Dinoflagellate Cysts and Palynomorphs

Here a variety of in this research encountered dinoflagellates and palynomorphs are detailed, of which the genus or species could not be determined with certainty. These unknown types of dinocysts and palynomorphs were photographed using a Leica light microscope (model: 020-519.511 DMLB 100T), which was equipped with a Leica camera of the type MC120 HD.

cf. Batiacasphaera sp. A

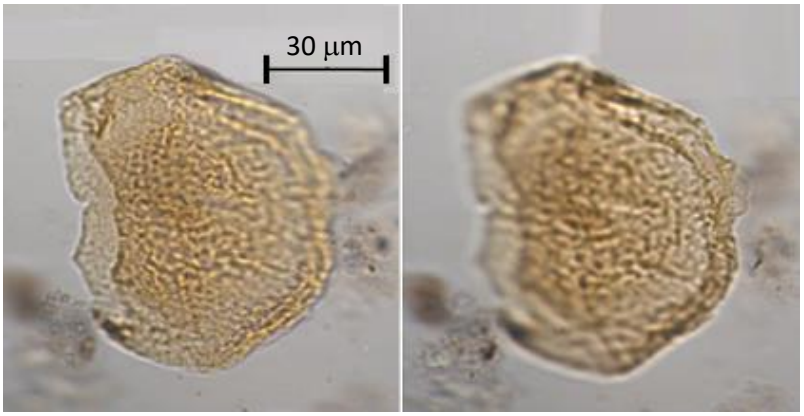

Figure 10: A specimen of *cf. Batiacasphaera sp. A* photographed in two different foci (400x zoom).

Synopsis: Light brown, dark yellow sub-spherical, slightly pentagonal shaped cysts of intermediate size, which does not bare septa, spines or processes. However its autophragm is ornamented with isolate or merged coarse ridges that appear to form some sort of maze network; the observed archaeopyles are exclusively large and apical with zigzag sutures.
Wall relationships: Presumably autophragm only.
Wall features: Proximate and reticulate cyst completely covered with isolate or merged coarse ridges of low relief that appear to form some sort of maze network, no septa, spines or processes were observed.
Paratabulation: Indicated by archaeopyle only, likely Gonyaulacoid due to archaeopyle.
Archaeopyle: Intercalary, Type : tA. Operculum free.
Paracingulum: Not observed.
Parasulcus: Only indicated by sulcal notch of archaeopyle.
Size: Intermediate, roughly 60-70 µm in diameter.
Stratigraphy: According to this study FO and LO observed in the early-Thanetian (sample N43-7 and N44-2).
Affinities: Possibly this is a species of *Batiacasphaera spp*., however no known species could be linked with the encountered specimens.

cf. Batiacasphaera sp. B

Figure 11: A specimen of *cf. Batiacasphaera sp. B* photographed in two different foci (400x zoom).

Synopsis: Small pale yellow-brown slightly elongated cysts, with a smooth to faintly reticulate proximate autopraghm; the observed archaeopyle is large and apical.
Wall relationships: Solely autophragm.
Wall features: Lacks septa, spines or processes, the phragm is smooth and faintly suggests fine scabrate features.
Paratabulation: Only expressed by archaeopyle, likely Gonyaulacoid due to archaeopyle.
Archaeopyle: Large and apical, type tA. Operculum free.
Paracingulum: Not observed.
Parasulcus: Only indicated by sulcal notch of archaeopyle.
Size: Small, approximately 30 µm long and 25-30 µm wide.
Stratigraphy: According to this study FO and LO observed in the mid-Thanetian (sample N44-6 to N44-8).
Affinities: Possibly this is a species of *Batiacasphaera spp*., however all to the researcher known species of this genus could not be linked with the described specimens and its size.

Operculodinium? cf. Fibrocysta

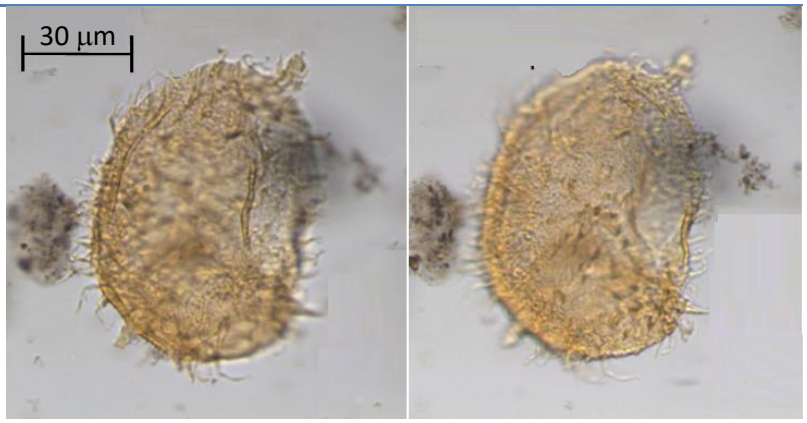

Figure 12: A specimen of *Operculodinium? Cf. Fibrocysta* photographed in two different foci (400 x zoom).

Synopsis: Skolochorate spherical to ovoid shaped cyst, which is densely covered with slender solid processes and bears a prominent apical and one or two sub-prominent antapical horns or projections. The phragm itself is fine granulate to punctoreticulate; the archaeopyle is large and precingular.
Wall relationships: Relative thick Autophragm, possibly double layered.
Wall features: Covered with nontabular solid processes of approximately one tenth of the central body diameter, which appear to be closed distally. One distinct apical and sometimes one or two antapical projections have been distinguished. The phragm between the processes is fine granulate to punctoreticulate.
Paratabulation: Besides archaeopyle not expressed , likely Gonyaulacoid due to archaeopyle on dorsal side of epicyst.
Archaeopyle: Prominent and precingular, operculum free.
Paracingulum: Only indicated by archaeopyle.
Parasulcus: Not observed.
Size: Intermediate, length 60-70 µm. Slightly longer than wide.
Stratigraphy: According to this study single occurrence in the late Danian was observed (sample N48-5).
Affinities: It resembles the genus *Operculodinium* in its wall features and by having a large precingular archaeopyle. Furthermore it resembles *Fibrocysta* in having distinct apical and/or antapical horns or projections.

Glaphyrocysta pastielsii ssp.reduced processes

Figure 13: A photographed specimen of *Glaphyrocysta pastielsii ssp. reduced processes (*400x zoom).

Synopsis: Spherical to sub-spherical murochorate cyst, with a densely covered network of trabeculae which generally lacks the central part of the process. Further ornamentation is not distinguished and the phragm itself appears to be smooth; an significant apical archaeopyle is observed.
Wall relationships: Autophragm only
Wall features: Dense cover of trabeculae which seem to originate from the paraplate margins. Moreover the central part of the trabeculae is strongly reduced/suppressed. The phragm indicates smoothness and is light brown to yellow in colour.
Paratabulation: Slightly indicated by supporting structures of the trabeculae and in combination with the apical archaeopyle the paratabulation may be classified as Gonyaulacoid.
Archaeopyle: Apical (possibly type tA, since the sulcal notch and other sutural features are generally well marked). Operculum free.
Paracingulum: Slightly indicated by supporting structures of the trabeculae.
Parasulcus: Sometimes indicated by sulcal notch in combination with supporting structures of the trabeculae.
Size: Intermediate to large. Diameter of central body roughly 90 µm.
Stratigraphy: Following the proposed age model of this studies, observed in the earliest Thanetian and in the latest Thanetian prior to the onset of the PETM (sample N45-1B and N42-2).
Affinities: Much alike the regular *Glaphyrocysta pastielsii* (e.g., Stover & Evitt, 1978) species, were it not for the fact that the central part of the Trabeculae processes are strongly reduced.

cf. Melitasphaeridium pseudorecurvatum

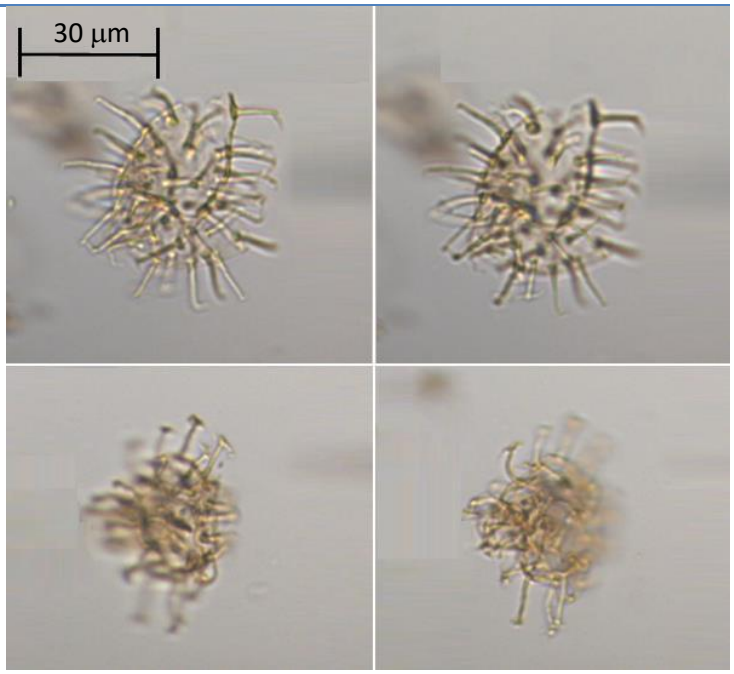

Figure 14: Two different specimens of *cf. Melitasphaeridium pseudorecurvatum* photographed in two different foci (400x zoom).

Synopsis: Small skolochorate egg-shaped cyst bearing typically one or two intratabular processes per paraplate. The tip of the processes tends to split into multiple stellate furcations, however in some specimens this furcation of the processes is less pronounced.
Wall relationships: Thin autophragm.
Wall features: Observed cysts contain one or two intratabular slender processes per paraplate, which are typically 10-15 microns in length. The ends of the processes tend to split into multiple stellate furcations and gives hints towards being open-ended. The base of the process are clearly observable. No septa or other wall features were observed.
Paratabulation: Not distinguished.
Archaeopyle: Unclear, due to position on cyst likely small apical.
Paracingulum: Not observed.
Parasulcus: Not observed.
Size: Small, roughly 25-35µm in length and around 20 µ wide.
Stratigraphy: Thrice observed in two samples which are dated to be early Thanetian (sample N44-8 and N45-1A).
Affinities: It resembles *Melitasphaeridium pseudorecurvatum* (e.g., Bujak et al., 1980) and weakly Cleistosphaeridium polypes (Davey, 1969a) due to its size the stellate furcations of the process-ends and the fact that the cysts bears one or two intratabular processes per paraplate.

Spiniferites? cf. celineae

Figure 15: A photographed specimen of *Spiniferites? cf. celineae* (400x zoom)

Synopsis: Light brown-yellow sub-spherical proximochorate cyst with a smooth to scabrate autophragm. It has low parasutural septa which are slightly elevated above the rest of the phragm. These septa bear small denticulate crests, which tend to be enlarged at gonal junctions. A precingular archaeopyle was observed.
Wall relationships: Only autophragm.
Wall features: At the parasutures low septa are formed, which bear small irregularly spread denticulate crest, which tend to be enlarged at gonal areas. Intratabularly the paraplates are smooth to scabrate.
Paratabulation: Is Gonyaulacoid and can be distinguished by the low parasutural septa.
Archaeopyle: Precingular
Paracingulum: can be distinguished by the low parasutural septa as well.
Parasulcus: can also be distinguished by the low parasutural septa.
Size: Small, 30-40 µm in diameter.
Stratigraphy: FO in an early Thanetian sample, hereafter multiple times encountered throughout the entire Thanetian interval (sample N42-2, N43-1, N44-2, N45-1A, N45-1B and N46-2B).
Affinities: Resembles *Impagidinium celineae* (e.g., du Chêne, 1988) in overall appearances and wall features, however the here described specimens are considerable smaller than *I. celineae* and display denticulations at the gonal junctions which presents hint toward the *Spiniferites* complex.

Palambages? sp.

Figure 16: Multiple specimens of *Palambages? sp.* photographed in two different zoomlevels (left and upper-right image: 400x zoom, and down-right image: 100x zoom).

Synopsis: Slightly transparent and light to dark brown colored sub-spherical to ovoidal microfossils that vary greatly in size. The fossils demonstrate a variety of openings in the studied specimens which sometimes resemble known dinocyst archaeopyles. However no consequent hole-shape can be observed from the fossils. These fossils are observed in a bloom that reached absolutes quantities of almost 56,000 specimens g^{-1} sample.

Wall relationships: Thin to moderately thick phragm.

Wall features: Slightly reticulate ornamentation can be observed apart from a relatively smooth surface.

Paratabulation: Not observed.

Archaeopyle: Some openings in the fossils resemble precingular, apical or intercalary archaeopyles

Paracingulum: Not observed

Parasulcus: Not observed

Size: Small to intermediate, 30- 120 µm

Stratigraphy: Single occurrence dated at the early to middle Selandian (sample N47-1A).

Affinities: The discovered fossils resemble the colony funghi *Palambages sp.* as described by Trivedi & Verma (1969) for instance, however the studied specimens do not show clear exclusive signs of colony forming.

Appendix D: Dinocyst Plates

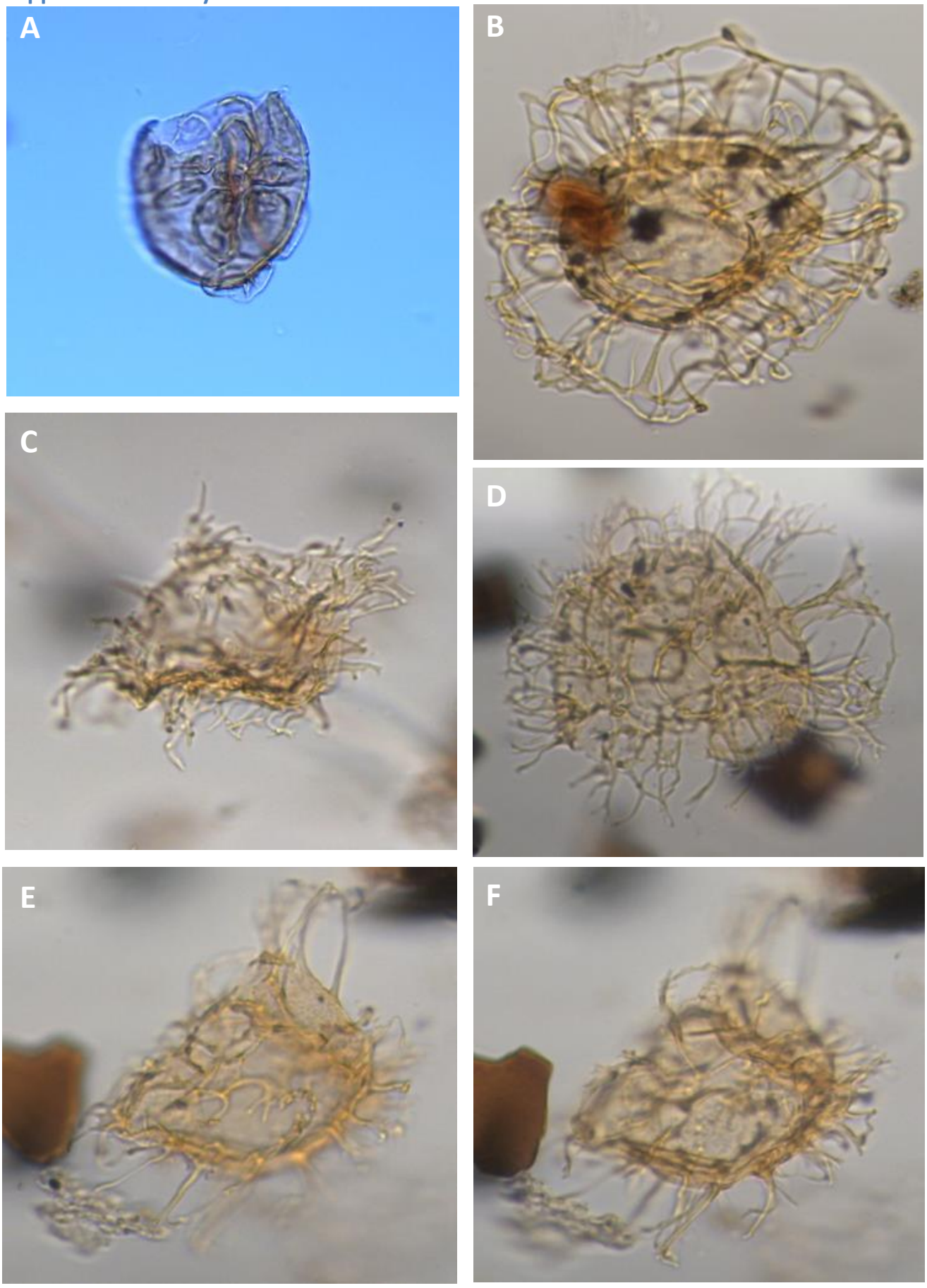

Plate I. **A**: *Alisocysta circumtabulata* 49R-3W, 64–66 cm; **B:** *Adnatosphaeridium multispinosum* 44R-6W, 119–121cm; **C:** *Apectodinium hyperacanthum* 44R-1W, 7–10 cm; **D:** *Areoligera cf. coronata* 46R-2W, 5–8 cm; **E & F:** *Areoligera gippingensis* 48R-2W, 5–8 cm

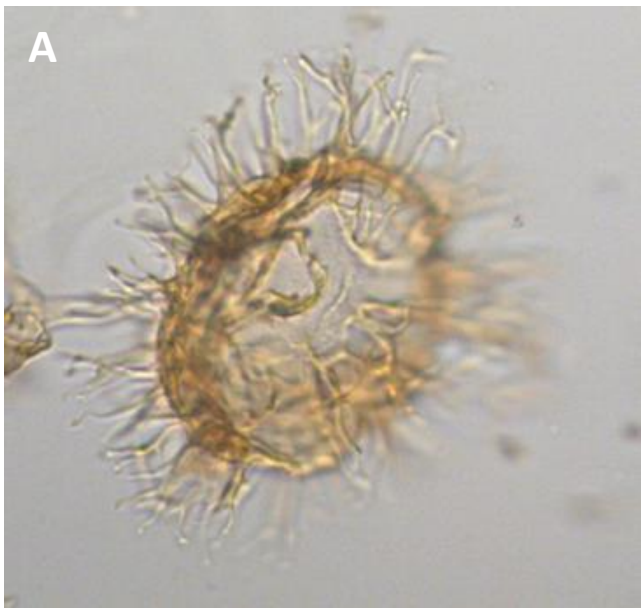

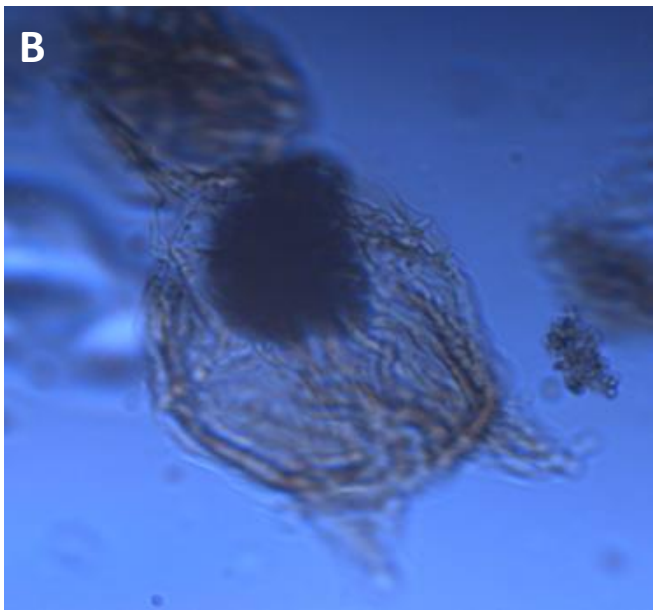

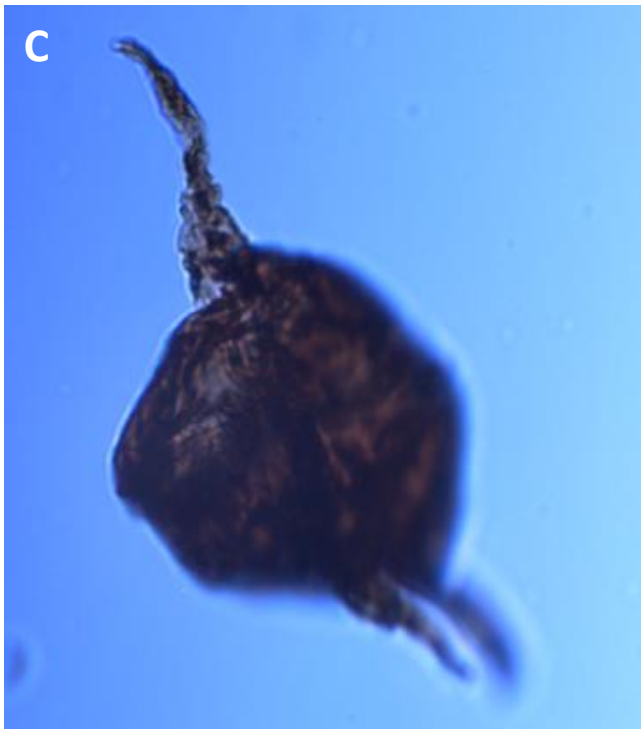

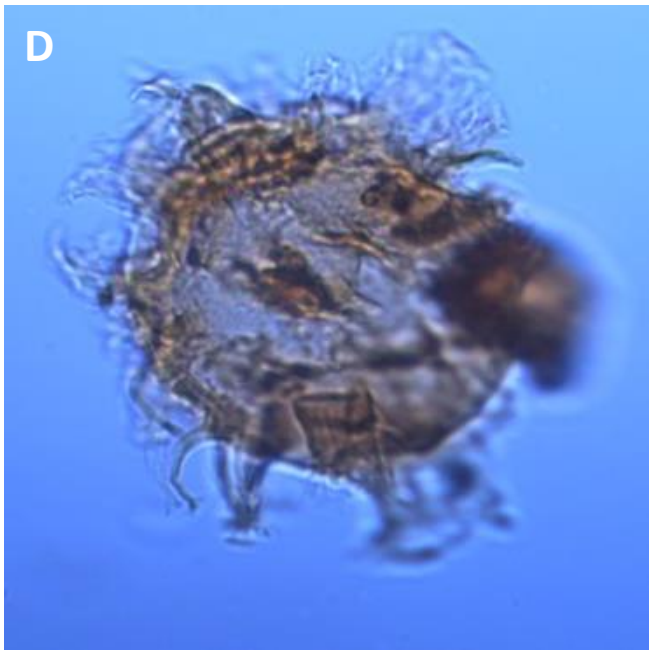

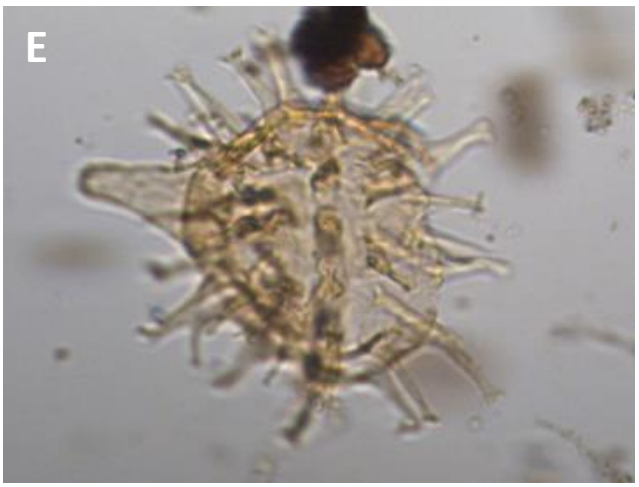

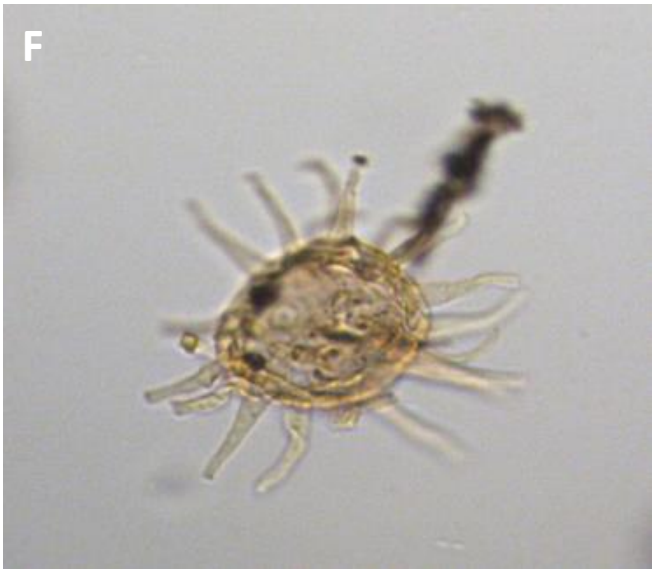

Plate II. **A**: *Areoligera cf. senonensis* 48R-4W, 53–55 cm; **B:** *Cerodinium medcalfii* 48R-3W, 50-53 cm; **C:** *Cerodinium diebellii* 49R-3W, 64–66 cm; **D:** *Damassidinium sp.* 49R-3W, 64-66 cm; **E:** *Diphyes colligerum* 48R-6W, 26-29 cm; **F:** *Dapsilidinium sp.* 49R-3W, 64-66 cm

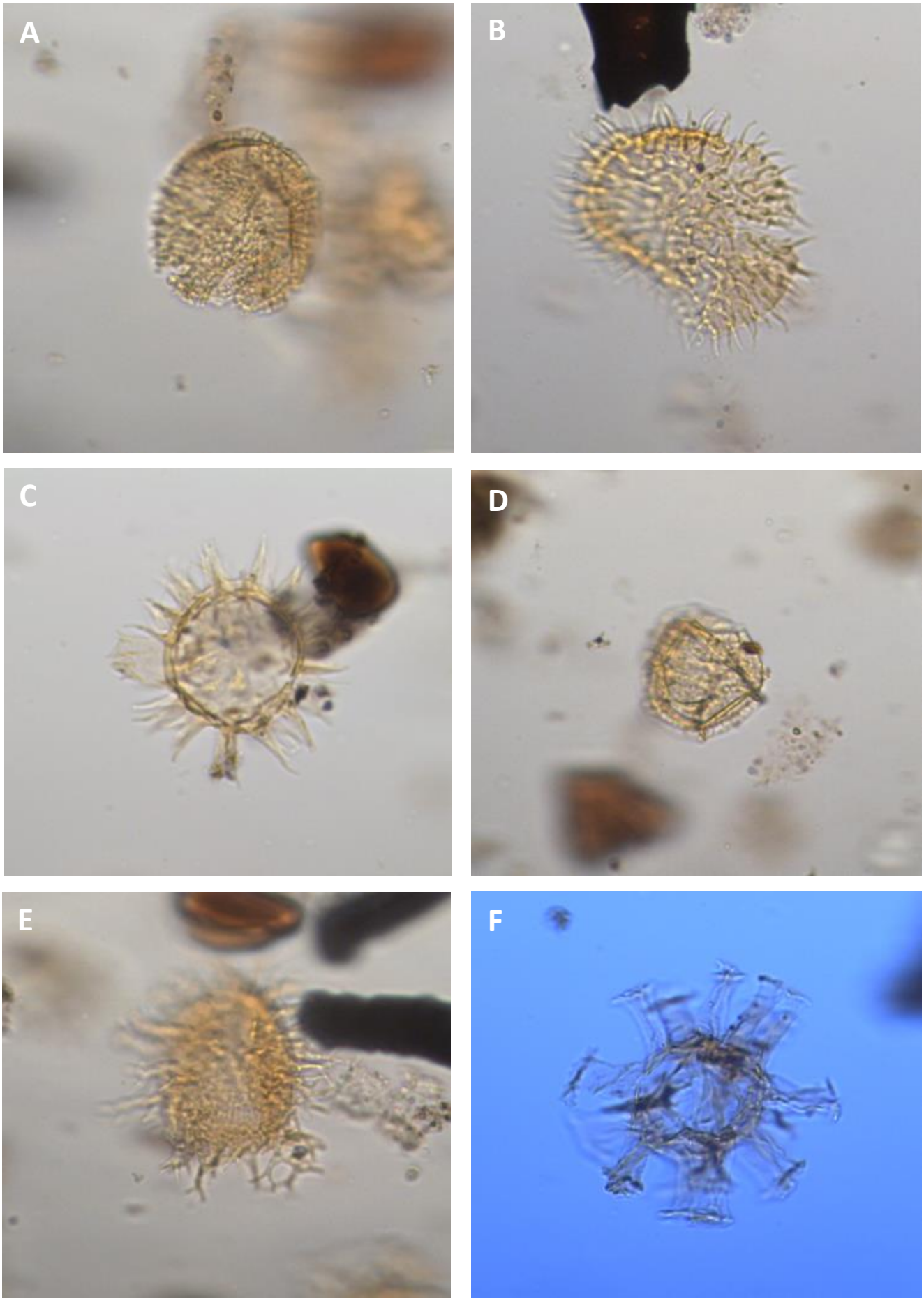

Plate III. **A**: *Elytrocysta druggii* 46R-2W, 5–8 cm; **B:** *Eocladopyxis peniculata* 43R-7W, 45-48 cm; **C:** *Florentinia reichartii* 44R-6W, 119–121 cm; **D:** *Fibradinium annetorpense* 48R-6W, 26-29 cm; **E:** *Hafniasphaera septata* 46R-2W, 5-8 cm; **F:** *Hystrichokolpoma rigaudiae* 49R-3W, 64-66 cm

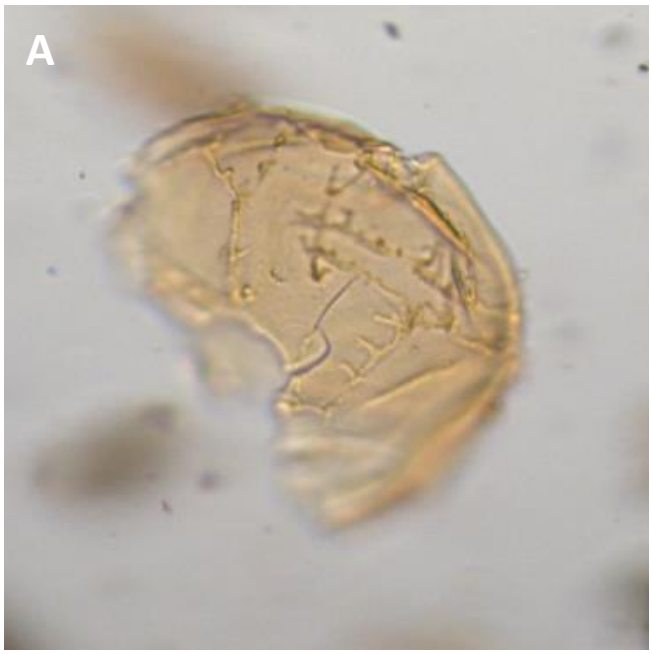

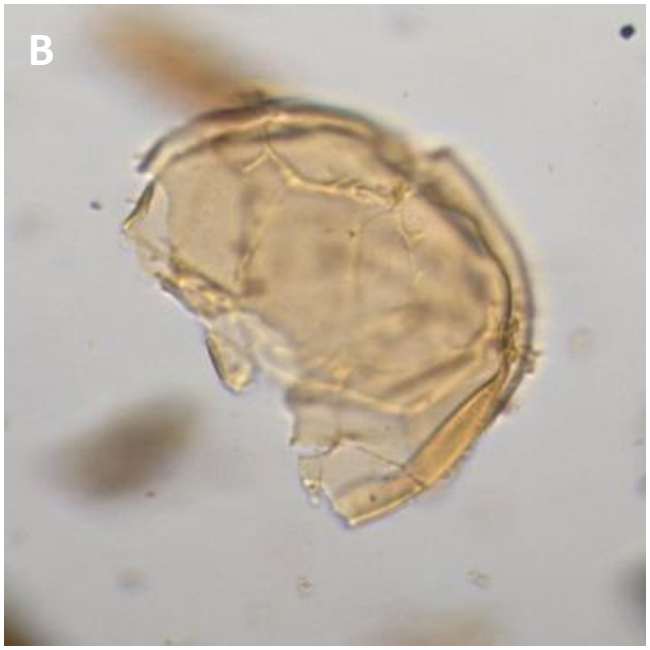

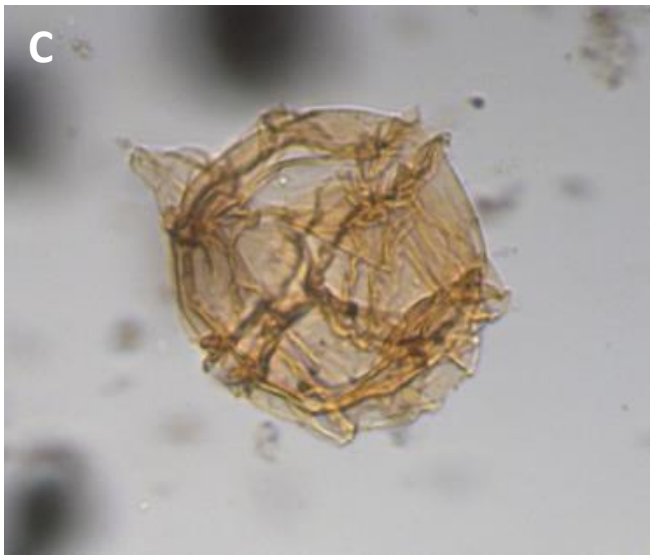

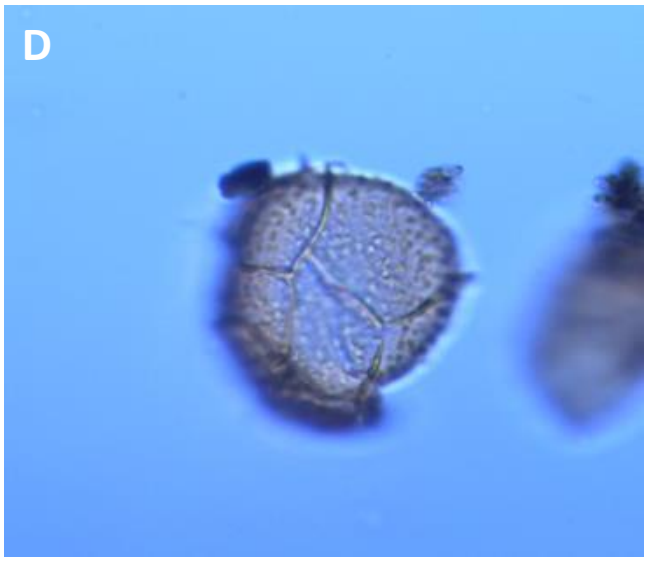

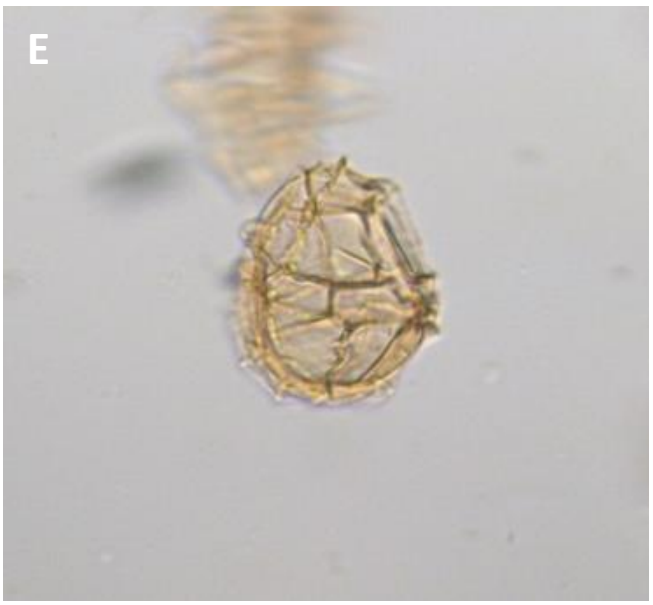

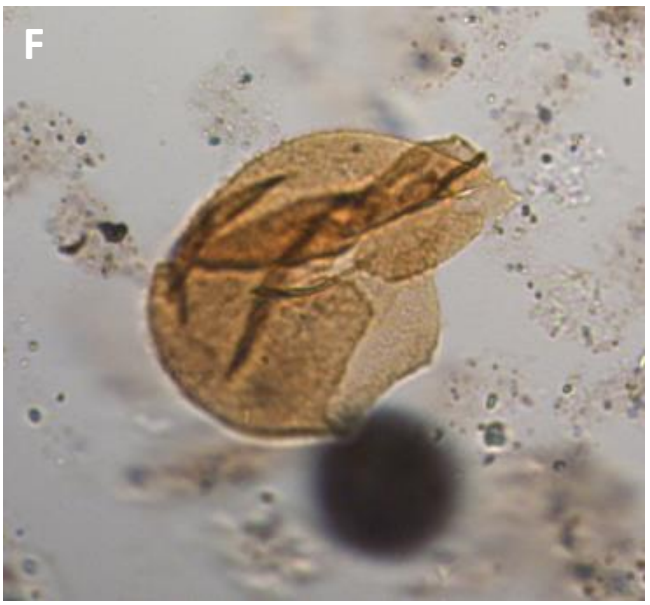

Plate IV. **A & B**: *Impagidinium celineae* 48R-2W, 67–70 cm; **C:** *Impagidinium aspinatum* 48R-5W, 78-81 cm; **D:** *Impagidinium maculatum* 49R-3W, 64-66 cm; **E:** *Impagidinium victorianum* 44R-8W, 41-44 cm; **F:** *Kallosphaeridium brevibarbatum* 43-7W, 45-48 cm

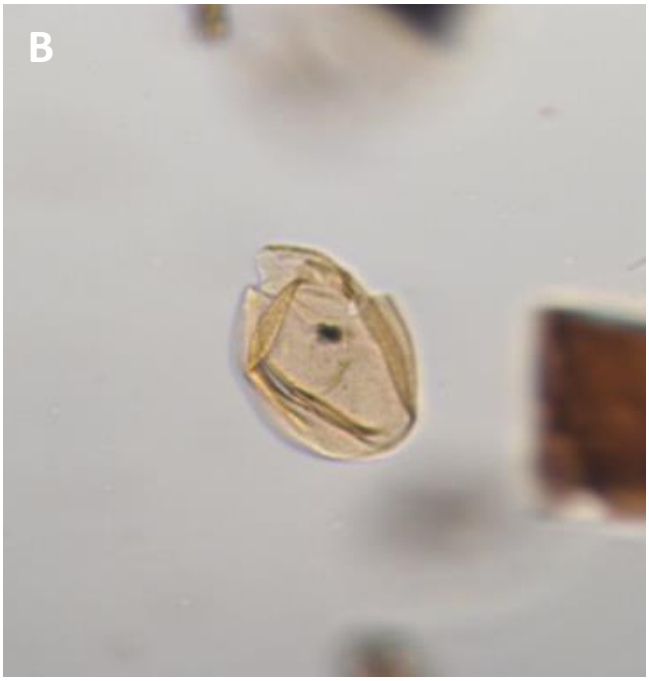

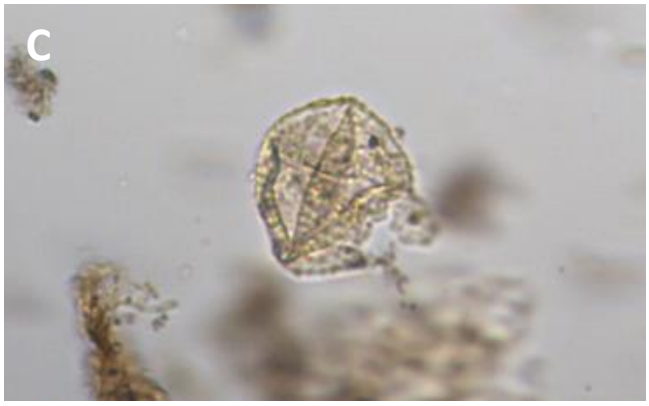

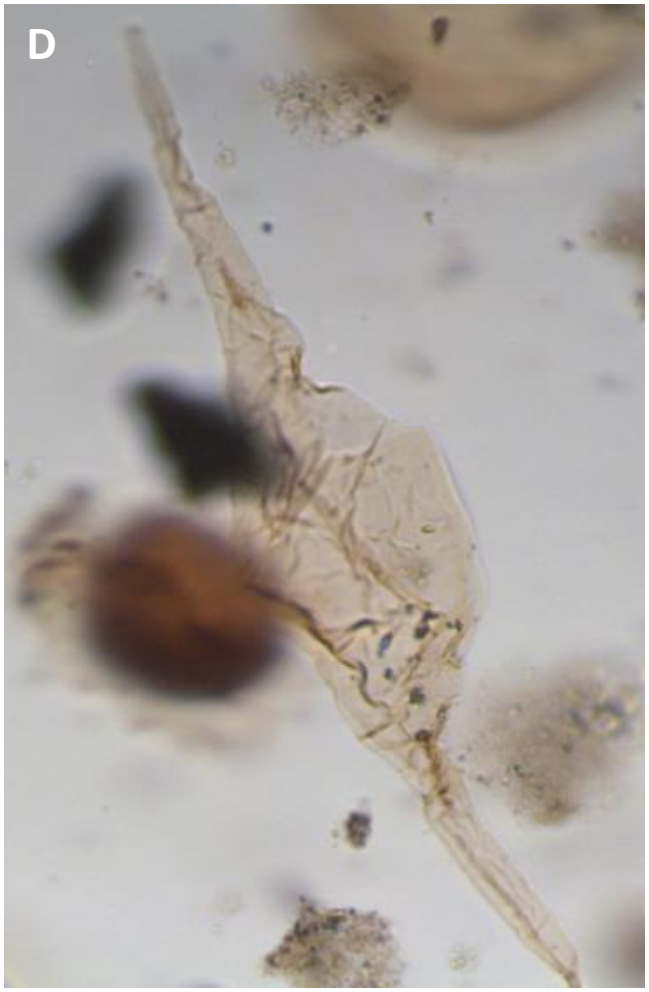

Plate V. **A**: *Kallosphaeridium granulatum* 46R-1W, 60–62 cm; **B:** *Kallosphaeridium yorubaense* 44R-6W, 119-121 cm; **C:** *Kallosphaeridium orchiesense* 48R-6W, 26-29 cm; **D:** *Palaeocystodinium golzowense* 48R-5W, 78-81 cm; **E:** *Palaeocystodinium australinum* 43-7W, 45-48 cm

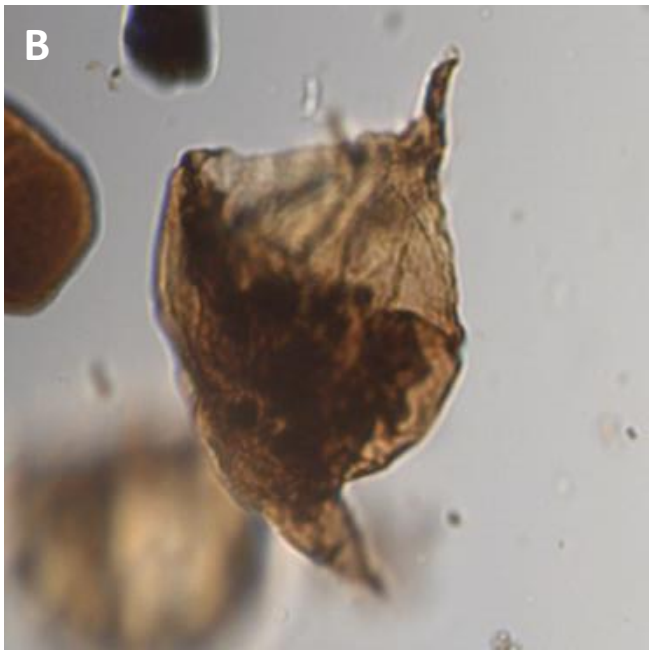

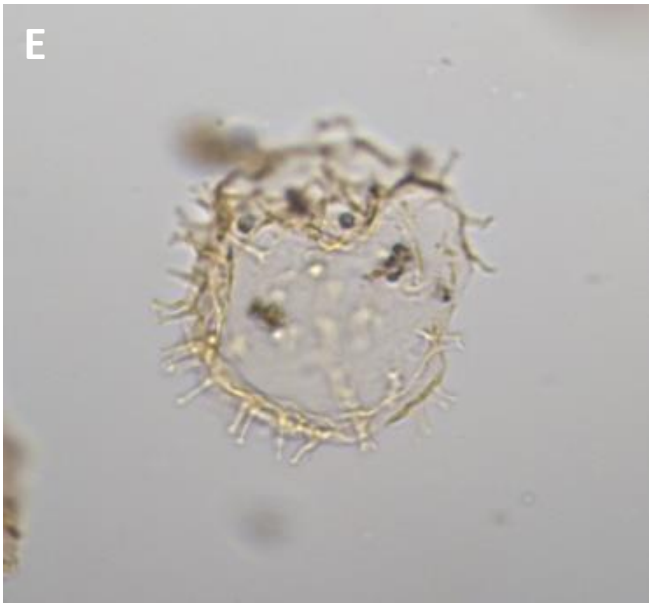

Plate VI. **A**: *Palaeocystodinium lidiae* 43R-7W, 45-48 cm; **B:** *Palaeocystodinium rafii / reductum* 49R-2W, 109-112 cm; **C:** *Phelodinium sp*. 49R-3W, 64-66 cm; **D:** *Pterodinium alectrolophum* 46R-1W, 60-62 cm; **E:** *Polysphaeridium zoharyi* 44-6W, 119-121 cm

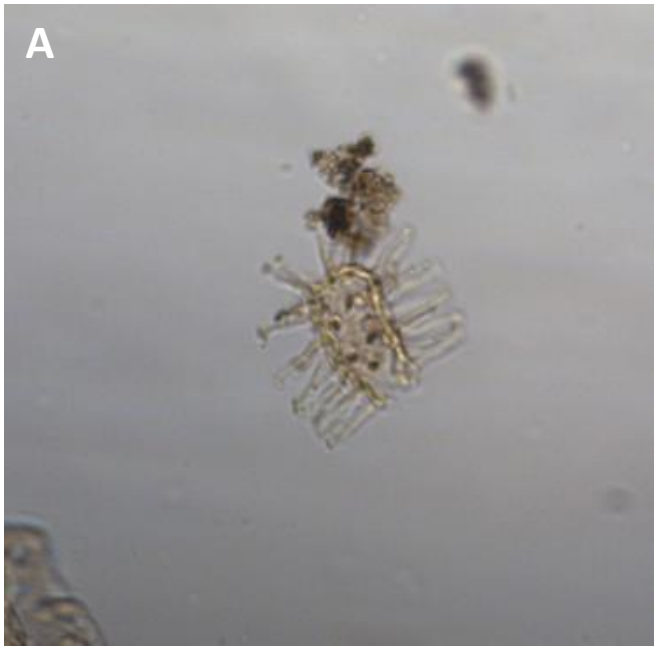

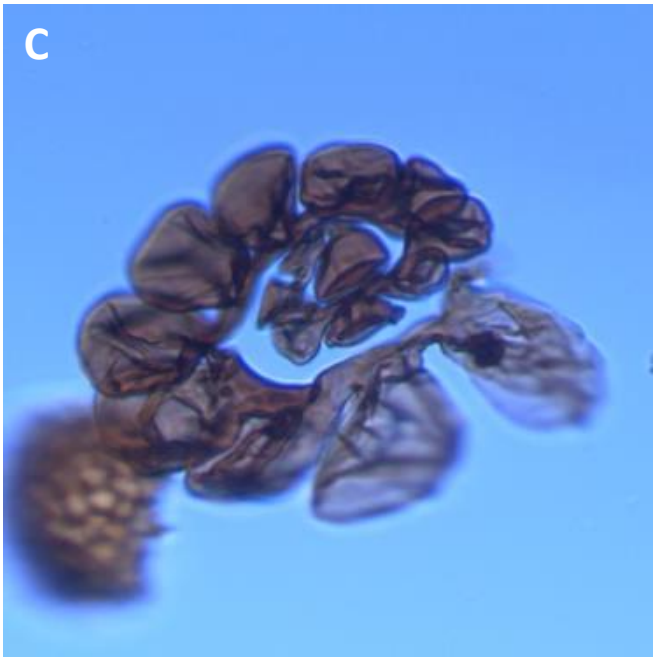

Plate VII. **A**: *Tanyosphaeridium xanthiopyxides* 49R-3W, 64-66 cm; **B:** *Trithyrodinium sp* 46R-2W, 5-8 cm;
C: *Foraminifera* lining. 48R-2W, 67-70 cm;

Appendix E: Statement of originality of the MSc thesis

I declare that:

1. This is an original report, which is entirely my own work,

2. Where I have made use of the ideas of other writers, I have acknowledged the source in all instances,

3. Where I have used any diagram or visuals I have acknowledged the source in all instances,

4. This report has not and will not be submitted elsewhere for academic assessment in any other academic course.

Student data:

Credentials:	Ing.
Name:	Mike Minze Nicolai
Registration number:	4290437
E-mail:	m.m.nicolai@students.uu.nl

Date: 27/08/2016

Signature:

References

Alberti, G. (1961). Zur Kenntnis mesozoischer und alteriorer Dinoflagellaten und Hystrichosphaerideen von Nord- und Mitteldeutschland sowie einigen anderen europaeische Gebieten. *Palaeontographica Abt. A*, *116*, 1–58.

Almogi-Labin, A., Bein, A., & Sass, E. (1993). Late Cretaceous upwelling system along the Southern Tethys margin (Israel): interrelationship between productivity, bottom water environments, and organic matter preservation. *Paleoceanography*, *8*.

Anand, P., Elderfield, H., & Conte, M. H. (2003). Calibration of Mg/Ca thermometry in planktonic foraminifera from a sediment trap time series. *Paleoceanography*, *18*, 21–28.

Archer, D. (2005). Fate of fossil fuel CO2 in geologic time. *Journal of Geophysical Research*, *110*(C09S05).

Artzner, D. G., & Dörhöfer, G. (1978). Taxonomic note: Lejeunecysta nom. nov. pro. Lejeunia Gerlach 1961 emend. Lentin and Williams 1976-dinoflagellate cyst genus. *Canadian Journal of Botany*, *56*(11), 1381–1382.

Below, R. (1982). Zur Kenntnis der Dinoflagellaten-Zysten Populationen im Ober Apt der Tongrube “Otto Gott” in Sarstedt/Norddeutschland. *Neu. Jahrb. Fuer Geol. Und Palaeont., Abhandlungen*, *164*, 339–363.

Benedek, P. N., & Gocht, H. (1981). Thalassisphora pelagica (Dinoflagellata, Tertiõr): electronenmikroskopische Untersuchung und Gedanken zur Palaeobiologie. *Palaeontographica Abt. A*, *180*, 39–64.

Biffi, U., & Grignani, D. (1983). Peridinioid dinoflagellate cysts from the Oligocene of the Niger Delta, Nigeria. *Micropaleontology*, *29*, 126–145.

Bignot, G. (1998). Middle Eocene benthic foraminifers from Holes 960A and 960C, central Atlantic Ocean. *Mascle, J., Lohman, G.P., Moullade, M. (Eds.), Proc. ODP Sci. Results*, *159*, 433–444.

Bijl, P. K., Houben, A. J. P., Schouten, S., Bohaty, S. M., Sluijs, A., Reichart, G., … Brinkhuis, H. (2010). Transient Middle Eocene Atmospheric CO2 and Temperature Variations, 5–7.

Bradford, M. R., & Wall, D. A. (1984). The Distribution of Recent Organic-Walled Dinoflagellate Cysts in the Persian Gulf, Gulf of Oman, and northwestern Arabian Sea. *Palaeontographica*, *192*.

Brinkhuis, H. (1994). Late Eocene to Early Oligocene dinoflagellate cysts from the Priabonian type-area (Northeast Italy): biostratigraphy and paleoenvironmental interpretation. *Palaeogeography, Palaeoclimatology, Palaeoecology*, *107*(1-2), 121–163. doi:10.1016/0031-0182(94)90168-6

Brinkhuis, H., Sengers, S., Sluijs, A., Warnaar, J., & Williams, G. L. (2003). Latest Cretaceous–earliest Oligocene and Quaternary dinoflagellate cysts, ODP Site 1172, East Tasman Plateau. *Proceedings of the Ocean Drilling Program, Scientific Results*, *189*, 1–48.

Brinkhuis, H., & Zachariasse, W. J. (1988). Dinoflagellate cysts, sea level changes and planktonic foraminifera across the Cretaceous-Tertiary boundary at El Haria, northwest Tunisia. *Marine Micropaleontology*, *13*.

Bujak, J. P., Downie, C., Eaton, G. L., & Williams, G. L. (1980a). Dinoflagellate cysts and acritarchs from the Eocene of southern England. *Special Papers in Palaeontology*, *24*, 100.

Bujak, J. P., Downie, C., Eaton, G. L., & Williams, G. L. (1980b). Taxonomy of some Eocene dinoflagellate cysts species from southern England.

Cleber, F. A. (2007). Cretáceo - Paleógeno da Bacia de Dahomey e Atlántico: Biostratigrafia, Paleocologia e Paleoceanografie dos Nanofósseis Calcários.

Cookson, I. (1965a). Cretaceous and Tertiary microplankton from the southeastern Australia. *Proc. of the Royal Soc. of Victoria*, *78*, 85–93.

Cookson, I. (1965b). Microplankton from the Paleocene Pebble Point Formation, south-western Victoria. *Proc. Roy. Soc. of Victoria*, *78*(1), 137–141.

Cookson, I., & Eisenack, A. (1961). Tertiary microplankton from the Rottnest Island Bore, Western Australia. *Journal of the Royal Society of Western Australia*, *44*, 39–47.

Cookson, I., & Eisenack, A. (1965). Microplankton from the Dartmoor Formation, SW. Victoria. *Proc. Roy. Soc. of Victoria*, *79*, 133–137.

Cookson, I., & Eisenack, A. (1974). Mikroplankton aus australischen Mesozoischen und Tertiõren Sedimenten. *Palaeontographica Abt. B*, *148*, 44–93.

Costa, L. I., & Downie, C. (1979). The Wetzeliellacaea; Palaeogene dinoflagellates. *Proceedings IV INternational Palynology Conference, Lucknow (1976-77)*, *2*, 34–46.

Crouch, E. M., Brinkhuis, H., Visscher, H., Adatte, T., & Bolle, M.-P. (2003). Late Paleocene-early Eocene dinoflagellate cyst records from the Tethys: Further observations on the global distribution of Apectodinium. *Special Paper of the Geological Society of America*, *369*, 113–131. doi:10.1130/0-8137-2369-8.113

Damassa, S. P. (1979). Eocene dinoflagellates from the Coastal Belt of the Franciscan Complex, northern California. *Journal of Palaeontology*, *53*, 815–840.

Davey, R. J. (1969a). Non-calcareous microplankton from the Cenomanian of England, northern France and North America, Part 1. *Bull. Brit. Mus (Nat. Hist.) Geol.*, *17*, 103–180.

Davey, R. J. (1969b). The evolution of certain Upper Cretaceous hystrichospheres from South Africa. *Palaeontologia Africana*, *12*, 25–51.

Davey, R. J., & Williams, G. L. (1966). The genus Hystrichosphaeridium and its allies. *Bull. Brit. Mus. (Nat. Hist.) Geol., Suppl.*, *3*, 53–106.

De Coninck, J. (1969). Dinophyceae et Acritarcha de l'Ypresien du Sondage de Kallo. *Mem. Inst. Roy. Sci. Nat. Belg., Brussels*, *161*, 1–67.

De Coninck, J. (1975). Microfossiles a paroi organique de l'Ypresien du Bassin belge. *Serv. Geol. Belge, Prof. Paper*, *12*, 1–151.

De Jonge, C., Hopmans, E. C., Stadnitskaia, A., Rijpstra, W. I. C., Hofland, R., Tegelaar, E., & Sinninghe Damsté, J. S. (2013). Identification of novel penta- and hexamethylated branched glycerol dialkyl glycerol tetraethers in peat using HPLC–MS2, GC–MS and GC–SMB-MS. *Organic Geochemistry*, *54*.

Deflandre, G. (1937). Microfossiles des Silex crétacés. 2. Flagellés incertae sedis, Hystrichosphaeridés, Sarcodinés. Organismes divers. *Masson*.

Deflandre, G., & Cookson, I. (1955). Fossil microplankton from Australian Late Mesozoic and Tertiary sediments. *Austal. Journal of Marine and Freshwater Research*, *6*, 242–313.

Drugg, W. S. (1967). Palynology of the Upper Moreno Formation (Late Cretaceous-Paleocene) Escarpado Canyon, California. *Palaeontographica Abt. B*, *120*, 1–71.

Du Chêne, J., & Adediran, S. A. (1984). Late Paleocene to early Eocene dinoflagellates from Nigeria. *Cahiers de Micropaléontologie*, *3*, 5–38.

Du Chêne, J. R. (1988). Étude sytématique des kytes de dinoflagellás de la Formation des Madeleines (Danien du Sénégal). *Cahiers de Micropaléontologie*, *2*.

du Chêne, J. R., Stover, L. E., & De Coninck, J. (1985). New observations on the dinoflagellate cyst genus Kallosphaeridium De Coninck, 1969. *Cahiers de Micropaléontologie*, *4*, 1–18.

Duxbury, S. (1980). Barremian phytoplankton from Speeton, east Yorkshire. *Palaeontographica Abt. B*, *173*, 107–146.

Eisenack, A. (1954). Mikrofossilien aus Phosphoriten des samländischen Unteroligozäns und über die Einheitlichkeit der Hystrichosphaerideen. *Palaeontographica Abt. A*, *105*, 49–95.

Eisenack, A. (1965). Über einige Mikrofossilien des samländischen und norddeutschen Tertiors. *Neues Jahrb. Für Geol. Und Pal., Abhandlunden*, *123*, 149–159.

Eisenack, A., & Gocht, H. (1960). Neue Namen für einige Hystrichosphaeren der Bernsteinformation Ostpreussens. *Neues Jahrb. Für Geol. Und Pal., Monatshefte*, 511–581.

Eshet, Y., Moshkovitz, S., Habib, D., Benjamini, C., Margaretz, M. (1992). Calcareous nannofossil and dinoflagellate stratigraphy across the Cretaceous/Tertiary boundary at Hor Hahar, Israel. *Mar. Micropaleontol 18*, 199-228.

Evitt, W. R., Damassa, S. P., & Albert, N. R. (1998). A tiger by the tail: the exophragm of the Cretaceous–Paleocene dinoflagellate Palaeoperidinium and its implications. *Palynology*, *22*.

Firth, J. V. (1996). Upper Middle Eocene to Oligocene dinoflagellate biostratigraphy and assemblage variations in hole 913B, Greenland Sea, in: Proceedings of the Ocean Drilling Program, Scientific Results.

Frieling, J., Gebhardt, H., Peterse, F., Reichart, G.-J., Sluijs, A., Huber, M., … Weste. (2016). *Climate, Carbon Cycling and Marine Ecology during the Paleocene-Eocene Thermal Maximum* (1st ed.). Zutphen: WPS.

Garrison, T. (2013). *Oceanography - An Invitation to Marine Sciences*. (A. Berg, Ed.) (8th ed.). Brooks/Cole.

Goodman, D. K., & Witmer, R. J. (1985). Archaeopyle variation and paratabulation in the dinoflagellate Diphyes colligerum (Deflandre and Cookson, 1955) Cookson, 1965. *Palynology*, *9*, 61–83.

Gradstein, F., Ogg, J., Schmitz, M., & Ogg, G. (2012). *The Geologic Time Scale 2012* (volume 2.). Munich: Elsevier B.V.

Guasti, E. (2005). Early Paleogene environmental turnover in the southern Tethys as recorded by formainiferal and organic-walled dinoflagellate cysts assemblages, 203.

Hansen, J. M. (1977). Dinoflagellate stratigraphy and echinoid distribution in Upper Maastrichtian and Danian deposits from Denmark. *Geological Society of Denmark, Bulletin*, *26*, 1–26.

Heilmann-Clausen, C. (1985). Dinoflagellate stratigraphy of the uppermost Danian to Ypresian in the Viborg 1 borehole, central Jylland, Denmark. *I Kommission Hos CA Reitzels Forlag*.

Hollis, C. J., Tayler, M. J., Andrew, B., Taylor, K. W., Lurcock, P., Bijl, P. K., & Phillips, A. (2014). Organic-rich sedimentation in the South Pacific Ocean associated with Late Paleocene climatic cooling. *Earth-Science Reviews*, *134*, 81–97.

Hopmans, E. C., Schouten, S., & Sinninghe Damsté, J. S. (2015). The effect of improved chromatography on GDGT-based palaeoproxies. *Organic Geochemistry*, *93*, 1–6. doi:10.1016/j.orggeochem.2015.12.006

Hopmans, E. C., Weijers, J. W., Schefuß, E., Herfort, L., Damsté, J. S. S., & Schouten, S. (2004). A novel proxy for terrestrial organic matter in sediments based on branched and isoprenoid tetraether lipids. *Earth and Planetary Science Letters*, *224*(1), 107–116.

Houben, S. (2008). Organic Walled Dinoflagellate Cysts as indicators for environmental change during the Middle Eocene Climatic Optimum (MECO): Results from ODP leg 120, Site 748 (Kerguelen Plateau). *Palaeoecology*, *29*.

Jolley, D. W. (1992). A new species of the dinoflagellate genus Areoligera Lejeune-Carpentier from the Late Paleocene of the eastern British Isles. *Tertiary Research*, *14*(1), 25–32.

Jolley, D. W., & Bell, B. R. (2002). The evolution of the North Atlantic Igneous Province and the opening of the NE Atlantic rift. *Geological Society, London, Special Publications*, *197*(1), 1–13.

Kim, J. H., van der Meer, J., Schouten, S., Helmke, P., Willmott, V., Sangiorgi, F., … Damst??, J. S. S. (2010). New indices and calibrations derived from the distribution of crenarchaeal isoprenoid tetraether lipids: Implications for past sea surface temperature reconstructions. *Geochimica et Cosmochimica Acta*, *74*(16), 4639–4654. doi:10.1016/j.gca.2010.05.027

Kim, J.-H. S., Schouten, E. C., Hopmans, B., Donner, J. S., & Damsté, S. (2008). Global sediment core-top calibration of the TEX86 paleothermometer in the ocean. *Geochimica et Cosmochimica Acta*, *72*.

Klumpp, B. (1953). Beitrag zur Kenntnis der Mikrofossilen des mittleren und oberen Eozõn. *Palaeontographica Abt. B*, *103*, 377–406.

Lear, C. H., Rosenthal, Y., & Slowey, N. (2002). Benthic foraminiferal Mg/Ca-paleothermometry: A revised core-top calibration. *Geochimica et Cosmochimica*, *66*, 3375–3387.

Lejeune-Carpentier, M. (1938). L'Étude microscopique des silex. Areoloigera: nouveau genre d'Hytrichospaeridée. *Annales Soc. Geol. Belgique*, *62*, 163–174.

Lejeune-Carpentier, M., & Sarjeant, W. A. S. (1981). Restudy of some larger dinoflagellate cysts and an acritarch from the Upper Cretaceous of Belgium and Germany. *Annales Soc. Geol. Belgique*, *104*, 1–39.

Lentin, J. K., & Williams, G. L. (1976). A monograph of fossil peridinioid dinoflagellate cysts. *BIO Report Series*, *75*(16), 1–237.

Lentin, J. K., & Williams, G. L. (1977). Fossil dinoflagellates: index to genera and species, 1977 edition. *BIO Report Series*, *77*(8), 1–209.

Malloy, R. E. (1972). An Upper Cretaceous dinoflagellate cyst lineage from Gabon, West Africa. *Geoscience and Man*, *4*, 57–65.

Mascle, J., Lohmann, G. P., & Clift, P. D. (1996). Proceedings of the Ocean Drilling Program, Initial Reports, Vol. 159, *159*, 65–150.

Masure, E., Rauscher, R., Dejax, J., Schuler, M., & Ferré, B. (1998). Cretaceous-Paleocene palynology from the Côte d'Ivoire-Ghana transform margin, sites 959, 961 and 962. *Proceedings of the Ocean Drilling Program, Scientific Results*, *159*, 433–444.

May, F. E. (1980). Dinoflagellate cysts of the Gymnodiniaceae, Peridiniaceae, and Gonyalacaceae from the Upper Cretaceous Monmouth Group, Atlantic Highlands, New Jersey. *Palaeontographica Abt. B*, *172*, 10–116.

McLean, D. M. (1976). Eocladopyxis peniculatum Morgenroth, 1966, Early Tertiary ancestor of the modern dinoflagellate Pyrodinium Bahamense Plate, 1906. *Micropaleontology*, *22*, 347–351.

Morgenroth, P. (1966). Mikrofossilien und Konkretionen des nordwest- europischen Untereozõns. *Palaeontographica Abt. B*, *119*, 1–53.

Morgenroth, P. (1968). Zur Kenntnis der Dinoflagellaten und Hystrichosphaeridien des Danien. *Geologisches Jahrbuch*, *86*, 533–578.

Norvick, M. S., & Burger, D. (1976). Mid-Cretaceous microplankton from Bathurst Island; in Palynology of the Cenomanian of Bathurst Island, Northern Territorv, Australia; Australian Bureau of Mineral Resources. *Geology and Geophysics*, *151*, 21–113.

Oboh-Ikuenobe, F. E. (1997). Palynofacies analysis of sediments from the CIG Transform Margin preliminary correlation with some regional events in the Equatorial Atlantic. *Palaeogeography, Palaeoclimatology, Palaeoecology*, *129*, 291–314.

Peterse, F., van der Meer, J., Schouten, S., Weijers, J. W. H., Fierer, N., Jackson, R. B., … Sinninghe Damsté, J. S. (2012). Revised calibration of the MBT-CBT paleotemperature proxy based on branched tetraether membrane lipids in surface soils. *Geochimica et Cosmochimica Acta*, *96*, 215–229. doi:10.1016/j.gca.2012.08.011

Pross, J., & Brinkhuis, H. (2005). Organic-walled dinoflagellate cysts as paleoenvironmental indicators in the Paleogene ; a synopsis of concepts. *Paläontologische Zeitschrift*, *79*, 53–59.

Reichart, G.-J., Brinkhuis, H., Huiskamp, F., & Zachariasse, J. W. (2004). Hyper-stratification following glacial overturning events in the northern Arabian Sea. *Paleoceanography*, *19*.

Rossignol, M. (1962). Analyse pollinique de sédiments marins Quaternaires en Israël. *Éditions Du Muséum*.

Rossignol, M. (1964). Hystrichosphaeres du Quaternaire en Méditerrane orientale, dans les sédiments actuelles. *Revue de Micropaléontologie*, *7*, 83–99.

Ruddiman, W. F. (2014). *Earth's Climate – Past and Future* (3rd ed.). New York: W. H. Freeman.

Sarjeant, W. A. S. (1966). Dinoflagellate cysts with Gonyaulax-type tabulation, 107–156.

Sarjeant, W. A. S. (1970). The genus Spiniferites Mantell, 1850 (Dinophyceae). *Grana*, *10*, 74–78.

Sarjeant, W. A. S. (1981). A restudy of some dinoflagellate cyst holotypes in the University of Kiel collections II. The Eocene holotypes of Barbara Klumpp (1953). *Meyniana*, *33*, 97–132.

Sarjeant, W. A. S. (1985). A restudy of some dinoflagellate cyst holotypes in the University of Kiel Collections: VI. Late Cretaceous dinoflagellate cysts and other palynomorphs in the O. Wetzel collection. *Meyniana*, *37*, 129–185.

Schiøler, P., & Wilson, G. (1993). Maastrichtian dinoflagellate zonation in the Dan Field, Danish North Sea. *Review of Palaeobotany and Palynology*, *78*(3).

Schouten, S., Hopmans, E. C., Schefuß, E., & Sinninghe Damsté, J. S. (2002). Distributional variations in marine crenarchaeotal membrane lipids: a new tool for reconstructing ancient sea water temperatures? *Earth and Planetary Science Letters*, *204*.

Shafik, S., Watkins, D. K., & Shin, I. C. (1998). Calcareous Nannofossil Paleogene Biostratigraphy , Côte D ' Ivoire-Ghana marginal ridge, Eastern Equatorial Atlantic. *Proceedings of the Ocean Drilling Program, Scientific Results*, *159*(1985), 413–431.

Slimani, H., Louwye, S., Toufiq, A. (2010). Dinoflagellate cysts from the Cretaceous–Paleogene boundary at Ouled Haddou, southeastern Rif, Morocco: biostratigraphy, paleoenvironments and paleobiogeography. *Palynology 34*, 90-124.

Sluijs, A., & Brinkhuis, H. (2009). A dynamic climate and ecosystem state during the Paleocene-Eocene Thermal Maximum – inferences from dinoflagellate cyst assemblages at the New Jersey Shelf. Biogeosciences Discussions, 6(3), 5163–5215. doi:10.5194/bgd-6-5163-2009

Sluijs, A., Brinkhuis, H., Crouch, E. M., John, C. M., Handley, L., Munsterman, D., … Dickens, G. R. (2008). Eustatic variations during the Paleocene-Eocene greenhouse world. *Paleoceanography*, *23*(4), 1–18. doi:10.1029/2008PA001615

Sluijs, A., Brinkhuis, H., Stickley, C. E., & Fuller, M. (2003). Dinoflagellate cysts from the Eocene-Oligocene transition in the Southern Ocean: Results from ODP Leg 189. *Proc. Ocean Drill. Program Sci. Results*, *189*(42).

Sluijs, A., Brinkhuis, H., Williams, G. L., & Fensome, R. A. (2009). Taxonomic revision of some Cretaceous-Cenozoic spiny organic-walled peridiniacean dinoflagellate cysts. *Review of Palaeobotany and Palynology*, *154*(1-4), 34–53. doi:10.1016/j.revpalbo.2008.11.006

Sluijs, A., Pross, J., & Brinkhuis, H. (2005). From greenhouse to icehouse; organic-walled dinoflagellate cysts as paleoenvironmental indicators in the Paleogene. *Earth-Science Reviews*, *68*(3-4), 281–315. doi:10.1016/j.earscirev.2004.06.001

Sluijs, A., Röhl, U., Schouten, S., Brumsack, H.-J., Sangiorgi, F., Sinninghe Damsté, J. S., & Brinkhuis, H. (2008). Arctic late Paleocene–early Eocene paleoenvironments with special emphasis on the Paleocene-Eocene thermal maximum (Lomonosov Ridge, Integrated Ocean Drilling Program Expedition 302). *Paleoceanography*, *23*.

Solomon, S., Qin, D., Manning, M., Marquis, M., Averyt, K., Tignor, M. M. B., … Chen, Z. (2007). *Climate Change 2007: The Physical Science Basis Contribution of Working Group I to the Fourth Assessment Report of the Intergovernmental Panel on Climate Change*. Cambridge (UK), New York (USA).

Stanley, E. A. (1965). Upper Cretaceous and Palaeocene plant microfossils and Paleocene dinoflagellates and hystrichosphaerids from southwestern Dakota,. *Bull. Amer. Paleont.*, *6*, 1–18.

Stockmarr, J. (1971). Tablets with spores used in absolute pollen analysis. *Pollen et Spores*, *13*, 615–631.

Stover, L. E., & Evitt, W. R. (1978). Analyses of pre-Pleistocene organic-walled dinoflagellates. *Stanford Univ. Publ., Geol. Sc.*, *15*, 1–300.

Stover, L. E., Riding, J. B., & Brinkhuis, H. (1996). *Mesozoic-Tertiary dinoflagellates, acritarchs and prasinophytes*. *Palynology: principles and applications* (Vol. 2).

Trivedi, B. S., & Verma, G. L. (1969). Fungal remains from Tertiary coal bed of Malaya. Journal of Palynology. *Journal of Palynology*, *5*(2).

Wagner, T. (2002). Late Cretaceous to early Quaternary organic sedimentation in the eastern Equatorial Atlantic. *Palaeogeography, Palaeoclimatology, Palaeoecology*, *179*, 113–147.

Wall, D. A. (1967). Fossil microplankton in deep-sea cores from the Caribbean Sea. *Palaeontology*, *10*, 95–123.

Wall, D., Dale, B., Lohmann, G.P., and Smith, W.K. (1977). The environmental and climatic distribution of dinoflagellate cysts in modern marine sediments from regions in the north and south Atlantic Oceans and adjacent seas. *Marine Micropaleontology*, v. 2, p. 121-200.

Weijers, J. W. H., Schouten, S., Spaargaren, O. C., & Sinninghe Damsté, J. S. (2006). Occurrence and distribution of tetraether membrane lipids in soils: Implications for the use of the TEX86 proxy and the BIT index. *Organic Geochemistry*, *37*(12), 1680–1693. doi:10.1016/j.orggeochem.2006.07.018

Westerhold, T., Röhl, U., Donner, B., McCarren, H. K., & Zachos, J. C. (2011). A complete high-resolution Paleocene benthic stable isotope record for the central Pacific (ODP Site 1209). *Paleoceanography*, *26*(PA2216).

Westerhold, T., Röhl, U., & Raffi, I. (2008). Astronomical calibration of the Paleocene time. *Palaeoecology*, *257*, 377–403.

Wetzel, O. (1933). Die in organischer Substanz erhaltenen Mikrofossilien des baltischen Kreide-Feuersteins mit einem sediment-petrographischen und stratigraphischen Anhang. *Palaeontographica Abt. A*, *78*, 1–110.

Williams, G. L., & Downie, C. (1966). Further dinoflagellate cysts from the London Clay. *Bull. Brit. Mus. (Nat. Hist.) Geol., Suppl.*, *3*(135-215).

Wilson, G. J. (1988). Paleocene and Eocene dinoflagellate cysts from Waipawa, Hawkes Bay, New Zealand. *Geological Survey Paleontological Bulletin*, *57*, 96.

Zachos, J. C., Stott, L. D., & Lohmann, K. C. (1994). Evolution of early Cenozoic marine temperatures at the Equator. *Paleoceanography*, *9*.